https://doi.org/10.5194/egusphere-2025-6235
Preprint. Discussion started: 12 January 2026

Phytoplankton community structure responses to episodic summer storms in a temperate coastal ecosystem

Harshal Chavan[1], Urania Christaki[1], Luis Felipe Artigas[1], Francois G. Schmitt[1]

[1]Université du Littoral Côte d'Opale, CNRS, Université de Lille, UMR 8187 LOG, 32 Ave. FOCH, 62930, Wimereux, France

Correspondence to: Harshal Chavan (harshal.chavan@univ–littoral.fr)

Abstract. Extreme events potentially modify the physical and biogeochemical environment resulting in dramatic changes of phytoplankton community structure. In this study the impact of 10 well identified storms on phytoplankton communities was explored in a productive coastal temperate ecosystem, the eastern English Channel (EEC). We focussed in summer because it is a low nutrient season where phytoplankton major shifts and blooms are not expected. Low-frequency (weekly to fortnightly) flow cytometry measurements of phytoplankton abundance were combined with high-frequency meteorological data (precipitation and wind) and hydrological records from 2012 to 2022. Storm impacts occurred in three distinct forms: high river inflow events, high wind stress–low inflow events, and low wind stress–low inflow events. High inflow storms, whether accompanied by weak or strong winds, promote coastal advection of riverine plumes enriched in nutrients, sustaining diatom dominance and, under high wind stress, favouring nano-sized phytoplankton (nanophytoplankton and cryptophytes). In contrast, low inflow conditions limit riverine nutrient supply, shifting reliance to regenerated nutrients from vertical mixing. When combined with strong winds, these conditions support nanophytoplankton growth, while short, low-wind storms favour pico-sized phytoplankton (*Synechococcus* spp. and picoeukaryotes). Across years, storms repeatedly reset seasonal succession and maintained environmental heterogeneity, leading to transient monospecific peaks of phytoplankton. These findings highlight storms as recurrent structuring forces in the EEC, mediating nutrient availability and driving shifts in phytoplankton composition across the summer months.

1 Introduction

The coastal marine ecosystems are vulnerable to changes in weather patterns and various extreme events, such as storms and heatwaves. The impact of extreme events can lead to deoxygenation, eutrophication, or the formation of harmful algal blooms in aquatic systems (Bianucci et al., 2018; Carpenter et al., 2022; Stockwell et al., 2020). Existing studies in lakes and oligotrophic seas in tropical and subtropical regions showed an increase in the Chl-a (chlorophyll-a) with cooling of the sea surface temperature (Babin et al., 2004; Jena et al., 2012) usually lasting for 1–3 weeks following storm passage and inducing changes in phytoplankton composition by altering seasonal succession (Thyssen et al., 2014). At higher latitudes, storm forcing has been associated with enhanced primary productivity; for example, Pozdnyakov et al., (2014) observed appreciable Chl-a increase in oligotrophic Arctic waters within days of a cyclone, while Crawford et al., (2020) reported elevated net primary production in inflow regions such as the Barents and southern Chukchi Seas. Despite these insights, the responses of rapidly changing temperate and high-latitude coastal seas to extreme events remain poorly resolved, particularly in terms of their influence on phytoplankton community structure. Most existing studies rely on Chl-a and derived productivity

https://doi.org/10.5194/egusphere-2025-6235
Preprint. Discussion started: 12 January 2026

estimates from satellite data (Crawford et al., 2020; Pozdnyakov et al., 2014; Zhao et al., 2009), yet the ecological consequences of storms are reflected not only on biomass but also on shifts in community composition and seasonal succession (Robache et al., 2025; Thyssen et al., 2014).

The English Channel is a temperate coastal sea generally characterized by strong atmospheric frontal activity and frequent extratropical storms, occasionally accompanied by thunderstorms. These systems typically originate in the North Atlantic and track towards north-western Europe, bringing prevailing south-westerly winds and enhanced precipitation (Kaspi and Schneider, 2013; Priestley et al., 2020; Priestley and Catto, 2022). With rising global temperatures, weakening of the polar midlatitude temperature gradient is reducing jet stream stability, leading to more persistent weather patterns and a higher frequency of extreme precipitation events in temperate regions (Crawford et al., 2023; Dietze et al., 2022; Francis et al., 2020; Pfleiderer et al., 2019). Within the English Channel, the eastern English Channel (EEC) is characterized by a nutrient-rich regime, particularly with an excess of nitrogen originating mainly from local rivers. The EEC coastline hosts numerous estuaries, including the Seine, the Somme, and several smaller systems such as the Authie, Canche, Liane, Wimereux, and Slack, which collectively contribute substantial nutrient inputs to coastal waters (Dulière et al., 2019). As a result, nutrient concentrations typically peak during the end of the winter leading to massive *Phaeocystis globosa* blooms in April–May each year (e.g., Breton et al., 2021; Lefebvre et al., 2011; Skouroliakou et al., 2022). By contrast, the end of spring is characterized by nutrient depletion, yet episodic summer blooms of diatoms as well as pico- and nano-sized phytoplankton have been observed (e.g., Houliez et al., 2023; Skouroliakou et al., 2022). Over recent decades, the summer season in the EEC has been increasingly dominated by pico-sized phytoplankton (Hubert et al., 2025a), accompanied by a decreasing trend in Chl-a concentrations (Hubert et al., 2025a; Huguet et al., 2024). Nevertheless, the causes of interannual variability in summer Chl-a concentrations and seasonal succession patterns remain poorly understood, reflecting the complex interplay among hydrodynamic processes, nutrient dynamics, and meteorological forcing. In a recent study (Skouroliakou et al., 2022), the summer phytoplankton succession in the EEC has been characterized as largely stochastic, with drift mechanisms accounting for more than 69% of community turnover. However, these authors did not identify specific environmental drivers underlying these stochastic processes. In the present work, we extend phytoplankton observations over a ten-year period and explore summer storm events as drivers of changes in phytoplankton composition.

The main objective of the present study was to better understand the occurrence of the summer phytoplankton blooms and in particular to investigate the possible effect of summer storm events on the magnitude of the blooms and also the phytoplankton community. We were particularly interested to examine how varying intensities of river inflow and wind affect phytoplankton community structure. We hypothesized that varying intensities of river inflow and wind drive distinct changes in abundance and community composition during otherwise more stable summer conditions. The phytoplankton community was characterized using size-based functional groups derived from flow cytometry along a coastal–offshore gradient in the Strait of Dover, known as the DYPHYRAD (Dynamics of PHYtoplankton on RADiale) transect (Hubert et al., 2025b) by the Strait of Dover. The dataset comprises 1835 samples collected on 268 dates during a ten-year survey (2012–2022). Storm characterization was based on Météo-France meteorological data (wind and precipitation) from the Boulogne-Sur-Mer station (https://meteo.data.gouv.fr/) and river discharge records from Eaufrance (https://www.eaufrance.fr/) near the DYPHYRAD transect. In this study, we examine phytoplankton community composition before and after storm

https://doi.org/10.5194/egusphere-2025-6235
Preprint. Discussion started: 12 January 2026

events, assess the various impacts of storms on the marine environment and phytoplankton structure, and conclude with a synthesis of our findings.

2 Materials and Method Section

2.1 Sampling strategy

The The eastern English Channel (EEC) is a shallow coastal sea where depths rarely exceed 50 m, with an average depth of 45 m between Calais and Dover (Fig. 1). The region is subject to macro- and mega-tidal regimes, with tidal amplitudes often surpassing 8 m, and it receives substantial nutrient inputs from multiple estuaries along the Picardy and Opale coasts, most notably the Seine, Somme, Authie, Canche, Liane, Wimereux, and Slack rivers (Fig. 1).

Phytoplankton data were collected between 2012 and 2022 as part of the DYPHYRAD transect (Dynamics of PHYtoplankton on RADiale; Hubert et al., 2025b). The transect spans approximately 9.7 km from coast to offshore and consists of nine stations ranging from R0 (50.8° N, 1.59° E) to R4 (50.8° N, 1.45° E) (Fig. 1). Sampling was performed aboard the research vessel Sepia II (CNRS INSU-FOF, Centre National de la Recherche Scientifique Institut National des Sciences de l'Univers–Flotte Océanographique Française). To facilitate analysis of spatial patterns, stations were categorized into two zones based on their proximity to shore: coastal (R0–R2) and offshore (R2′–R4). Sampling was conducted approximately weekly from February 2012 to December 2022, providing a long-term dataset suitable for both temporal and spatial analysis. Sampling was conducted approximately weekly from February 2012 to December 2022, providing a long-term dataset suitable for both temporal and spatial analyses. The DYPHYRAD network includes nine sampling stations, with the highest sampling frequency at station R1 (227 samples, Table 1). Additional details regarding data acquisition and validation are provided in Hubert et al. (2025b).

In addition to DYPHYRAD, we incorporated datasets from two French National Observation Systems (Systèmes Nationaux d'Observation, SNO): SNO SOMLIT and SNO Phytobs. SNO SOMLIT (Savoye et al., 2024) contributed data from two stations (SOMLIT C and SOMLIT L), sampled two to four times per month (Table 1). SNO Phytobs (Lemoine et al., 2024) provided data from two additional stations Wimereux (SOMLIT C) and Boulogne-1 also sampled two to four times per month. Data from the SOMLIT C and Phytobs stations were classified as coastal, whereas data from SOMLIT L were considered offshore. Phytobs station Wimereux and SNO SOMLIT C share the same location.

2.2 Nutrients and Chlorophyll-a

At each station (R0–R4), sea surface temperature (T, °C) and salinity (S, PSU) were measured using a conductivity-temperature-depth profiler (CTD Seabird SBE 25). Subsurface water samples were collected for dissolved inorganic nutrients (NO_2^-, NO_3^-, PO_4^{3-} and $Si(OH)_4$. Nutrient concentrations were quantified using an autoanalyzer (AutoAnalyzer ALLIANCE SpA, Italy until 2016; then AA3 HR AutoAnalyzer, SEAL Analytical GmbH, Germany) following a protocol based on Aminot and Kérouel, (2004). Chl-a concentrations were measured

https://doi.org/10.5194/egusphere-2025-6235
Preprint. Discussion started: 12 January 2026

using a Turner Designs 10-AU field fluorometer (Turner Designs Ltd, USA), as described in the equations developed by (Lorenzen, 1966).

SOMLIT SNO measurements used in this study include temperature, salinity, nutrients (nitrate, nitrite, phosphate, and silicate), all collected according to the standardized SOMLIT protocol. In addition to the DYPHYRAD transect, chlorophyll-a concentrations from the Phytobs stations (Wimereux SOMLIT-C and Boulogne-1) were included in the analysis to provide a broader overview of the EEC. Further details on environmental data acquisition and sample processing are available on the SOMLIT observation network website (https://www.somlit.fr/en/).

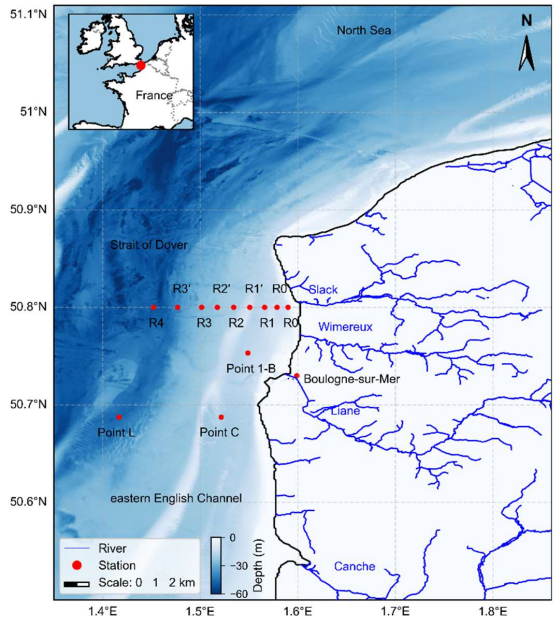

Figure 1. Map of the study area showing the locations of DYPHYRAD stations (R0–R4), SOMLIT stations (Point L and Point C), the Phytobs station Point 1 Boulogne (Point 1-B), and the Météo-France station Boulogne-Sur-Mer in the eastern English Channel near the Strait of Dover.

2.3 Phytoplankton abundance

The dataset comprises 1835 samples collected over 268 dates during a ten–year survey (2012–2022, Table 1). Single-cell optical analyses were conducted using pulse-shape recording flow cytometers (CytoSense and CytoSub, manufactured by CytoBuoy b.v., Woerden, Netherlands), which are designed for high-resolution in vivo characterization of phytoplankton based on their optical properties. Four cytometers were used over the 11-year time series. These instruments count particles ranging from 0.1 to 800 µm in width, covering practically the entire phytoplankton size range. Technical specifications for each flow cytometer are detailed in previous studies (Bonato et al., 2015, 2016; Hubert et al., 2025a; Louchart et al., 2020). Briefly, two protocols were employed: the "Pico" protocol used low detection thresholds (10mV red fluorescence), low pump speed (5µL s^{-1}), and short sampling time (5 min) to target 0.1–3 µm cells with low fluorescence and high abundance. The second protocol targeted nano- and microphytoplankton using higher detection thresholds (25mV red fluorescence), high pump speed (1013

https://doi.org/10.5194/egusphere-2025-6235
Preprint. Discussion started: 12 January 2026

µL s^{-1}), and longer sampling time (8–10min). The flow cytometers are equipped with a blue laser (488 nm, 50 mW) to allow discrimination between phototrophic and non-phototrophic particles. Cytogram analysis (biplots combining scatter and fluorescence data, Hubert et al., 2025a) was performed using CytoClus 4 software (CytoBuoy b.v., Netherlands). Phytoplankton functional groups (PFGs) were manually discriminated and characterized based on their size distribution, structural complexity, and fluorescence signals, following the interoperable vocabulary of (Thyssen et al., 2022). Five major phytoplankton groups were distinguished: picoeukaryotes (RedPico), nanophytoplankton (RedNano), microphytoplankton (mainly diatoms; RedMicro), *Synechococcus* spp. (OraPicoProk), and cryptophytes (OraNano) (Hubert et al., 2025a; Thyssen et al., 2022, Table 2).

Phytobs stations located south of the DYPHYRAD transect (50.8° N, Fig. 1) provide taxonomic information on diatoms, while SOMLIT stations supply additional pico- and nano-phytoplankton data. Bi-weekly microscopic counts from PHYTOBS Boulogne (Point 1-Boulogne) and Wimereux (SOMLIT-C) were used to identify dominant phytoplankton species in the study area. Additional datasets from SOMLIT stations C and L were used to compare pico- and nano-phytoplankton abundances with DYPHYRAD observations. These complementary observations were not included in the statistical analysis.

Table 1. Sampling stations and associated spatial, temporal, and sampling characteristics.

Station	Date	Longitude (° E)	Latitude (° N)	Distance from the coast (km)	Sampling frequency	Number of samples
R0	2012-2022	1.59	50.8	0.95	Once/twice a week	192
R0′		1.57	50.8	1.7		189
R1		1.56	50.8	2.6		227
R1′		1.55	50.8	3.7		164
R2		1.53	50.8	4.3		166
R2′		1.51	50.8	6.1		147
R3		1.50	50.8	7.3		150
R3′		1.47	50.8	9		137
R4		1.45	50.8	10.9		150
SOMLIT Point C		1.52	50.68	2	fortnightly	168
SOMLIT Point L		1.41	50.68	9.8		125
Phytobs Wimereux (SOMLIT C)		1.52	50.68	2		160
Phytobs 1-Boulogne		1.55	50.75	3.2		197

2.3 Storm event identification and characterization

Storm events were characterized using hourly measurements of wind speed, wind direction, and precipitation from the Météo–France Boulogne-Sur-Mer station (50.73° N, 1.59° E; https://meteo.data.gouv.fr/) for the period 2012–2022. The station is located 8 km from the DYPHYRAD transect. The 90th percentile threshold of wind speed was calculated from a 25-year reference period (1 January 2000 to 30 June 2025).

https://doi.org/10.5194/egusphere-2025-6235
Preprint. Discussion started: 12 January 2026

Table 2. Flow cytometry (FCM) phytoplankton group vocabulary and brief descriptions of the phytoplankton groups and their FCM characteristics in the eastern English Channel (adapted from Hubert et al., 2025 and Thyssen et al., 2022).

Phytoplankton groups	Phytoplankton description	Flow Cytometry characteristics
OraPicoProk (< 3 µm)	*Synechococcus* spp., unicellular photosynthetic cyanobacteria	Orange fluorescing prokaryote picophytoplankton, rich in the pigment phycoerythrin
RedPico (< 3 µm)	Picophytoplankton	Red only fluorescing picophytoplankton (not rich in phycoerythrin)
RedNano (≈ 3–20 µm)	Nanophytoplankton	Red only fluorescing nanophytoplankton (not rich in phycoerythrin)
OraNano (≈ 3–20 µm)	Larger cyanobacteria (e.g., large-size Crocosphaera, Richelia) red algae and cryptophytes	Orange and red fluorescing nanophytoplankton, rich in the pigment phycoerythrin
HsNano (≈ 3–20 µm)	Coccolithophores, and some autotrophs and armoured dinoflagellates	Red fluorescing nanophytoplankton with relatively high sideward light scattering properties
RedMicro (cells or chains > 20 µm)	Diatoms, and other microphytoplankton	Red only fluorescing microphytoplankton

Storm events in this study were identified as periods when wind speeds exceeded the 90th percentile (Fig. A1) (11.3 m s^{-1}). Storm length was initially identified as the ±3-day period surrounding the peak wind speed day, with day 3 designated as the storm day. Storms were selected for analysis when phytoplankton abundance and environmental data were available for at least 10 days prior to the storm day and for 14 days following the peak storm event. Wind observations include both wind speed and direction (Fig. A1–A2). Wind observations were used to evaluate the wind stress at the sea surface (τ, N m^{-2}) computed as (Wu, 1982):

$$\tau = \rho_{air} C_d U^2, \quad (1)$$

where ρ_{air} is the air density (assumed here as constant ρ_{air} = 1.225 kg m^{-3}) and the drag coefficient C_d was assumed to depend on the wind speed as (Wu, 1982):

$$C_d = (0.8 + 0.065U)\, 10^{-3} \quad (2)$$

The wind stress was derived from wind speed using a ±3-day window around each peak date. This approach allowed us to classify periods of low versus high wind forcing, which in turn served as an indicator of water column stability and the likelihood of wind-induced mixing.

Daily freshwater inflows were obtained from river discharge data for the Slack and Wimereux rivers, which border the transect (Fig. 1) (Eaufrance; https://www.eaufrance.fr). River flow rates were used as indicators of riverine inputs from the respective watershed areas. For the analysis, we used the combined inflow from both rivers to estimate the mean freshwater input during storm event. We expect phytoplankton to respond rapidly to changes in nutrient availability. In the study area, river plumes are transported under the influence of prevailing south–westerly winds. Consequently, the River Slack and the Wimereux estuary affect water chemistry along the transect earlier than other estuaries in the region (Fig. 1), thereby initiating changes in community structure. Total

https://doi.org/10.5194/egusphere-2025-6235
Preprint. Discussion started: 12 January 2026

precipitation (mm) and mean river inflow ($m^3 s^{-1}$) were calculated over the ±3-day storm period (Fig. 3). Thresholds for total precipitation and mean river flow were derived from the combined June–July distribution across the 25-year period (Fig. B1), with the 80th percentiles used to define "High" and "Low" classes as indicators of storm impact (Fig. 3). In addition, interannual variability in the number of windy days (wind speed > 8 m s^{-1}) and average river inflow ($m^3 s^{-1}$) from the Slack and Wimereux rivers during June and July near the DYPHYRAD transect was analyzed to characterize storm and freshwater input patterns (Fig. 4).

2.4 June–July baseline phytoplankton distribution

Whisker plots were constructed to evaluate post-storm changes in Chl-a and to examine variability in Chl-a relative to the average river discharge associated with each storm (Fig. 5). Due to the limited temporal coverage of Chl-a measurements in the DYPHYRAD dataset, Chl-a data from all available stations were used. These data were also employed to construct the seasonal climatology of Chl-a (Fig. C1c). Seasonal climatology of phytoplankton abundances were derived from DYPHYRAD data (Fig. 6). To assess the impact of storm events on phytoplankton abundances, we calculated the empirical complementary cumulative distribution function (CCDF, (Helton, 1997)), which represents the probability of observing abundance greater than or equal to a particular abundance level. In order to focus on all values, from medium to extremes, the CCDF were displayed in log–log plots to emphasize extreme events (Derot et al., 2015), (Fig. 7). For each phytoplankton group, the CCDF ($P(X \geq x)$) was constructed from June–July observations from the DYPHYRAD dataset, providing a baseline distribution:

$$P(X \geq x) = 1 - F_X(x) \quad (3)$$

Where $F_X(x)$ is the cumulative distribution function of a phytoplankton abundances X and x denotes a specific abundance threshold (i.e., an observed value of phytoplankton abundance).

Shaded percentile bands (50–90%) were used to represent the expected June–July baseline variability, and values falling outside this range were interpreted as extreme abundances (Fig. 7). Phytoplankton abundances from the pre-storm (−10 days) and post-storm (up to 14 days) periods were compared with this baseline to determine whether post-storm conditions remained within, or exceeded, the typical seasonal range. This non–parametric approach avoids assumptions about underlying distributions and is particularly suitable in this context, as phytoplankton abundances are not normally distributed (Derot et al; 2015). It also allows for a direct comparison of pre- and post-storm conditions relative to the seasonal climatology. Post-storm abundances were further examined using a distribution-wide Anderson-Darling test and a tail-focused exceedance test.

3 Results

3.1 Storm duration, precipitation and river flow rate

Based on the availability of flow cytometry data, ten storms were retained for analysis, each showing distinct patterns in wind stress, precipitation, and river inflow. Wind speeds above 8 m s^{-1} generated wind stress exceeding 0.1 N m^{-2} (Fig. 2), reaching more than 0.2 N m^{-2} during extreme winds (> 11.3 m s^{-1}). Several storms persisted for multiple days (e.g., 2016-07-02; Fig. A1), with the 2016-07-02 event representing the most intense episode, during which wind stress frequently surpassed 0.1 N m^{-2} (Fig. 2). Storm associated wind stress varied considerably among events (Fig. 2). Most storms were characterized by sustained windy conditions, with median and interquartile range (IQR) values close to 0.1 N m^{-2}, whereas others were weaker, marked only by short bursts of strong winds

https://doi.org/10.5194/egusphere-2025-6235
Preprint. Discussion started: 12 January 2026

(2016-06-22, 2020-06-06, 2022-06-06). The consistently windy storms included 2012-06-22, 2012-07-12, 2013-06-05, 2015-06-06, 2015-07-13, 2016-07-02, and 2020-07-27 (Fig. 2; Table 3). Across all events, wind speeds exceeding 8 m s^{-1} originated predominantly from south-westerly directions (Fig. A2).

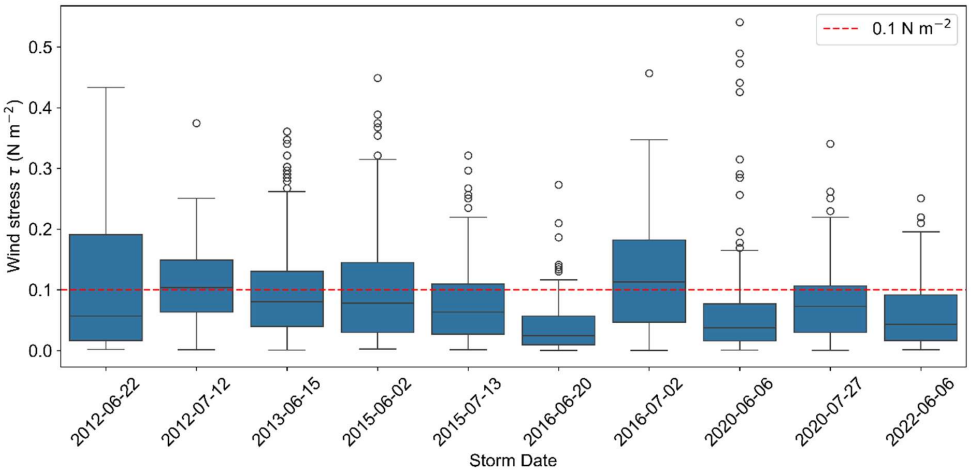

Figure 2. Wind stress (τ; N m^{-2}) across 10 storms, derived from wind speed over ±3 days around each storm. The red dashed line marks the 0.1 N m^{-2} threshold used to categorize storms as high or low wind stress.

Figure 3 presents total precipitation and average flow rate during each storm event. Precipitation amounts ranged from 1 mm (2015-07-13) to 32.20 mm (2016-06-20) over the ±3-day window surrounding each storm (Fig. 3a). "High" precipitation was defined as ≥ 16.12 mm, and "High" inflow as ≥ 0.45 m^3 s^{-1} (Fig. B1). In most cases, precipitation amounts corresponded with flow rates, with high precipitation events typically producing high inflows (Fig. 3). Exceptions included the 2020-07-27 and 2022-06-06 storms, where this relationship did not hold. Similarly, the 2016-07-02 storm showed low precipitation at Boulogne sur mer but was associated with elevated inflows (Fig. 3). Across all events, discharge ranged from a minimum of 0.18 m^3 s^{-1} (2015-07-13) to a maximum of 1.98 m^3 s^{-1} (2016-06-20).

River discharge strongly influenced salinity, which decreased below the climatological mean of 34.42 PSU during "High" inflow storms (Fig. C1b). Events in 2012, 2013, and 2016 were associated with elevated inflows and produced marked salinity reductions (33.4–34.0 PSU; Table 3). The highest discharge rate (1.976 m^3 s^{-1} on 2016-06-20) corresponded to the lowest observed salinity (33.4 PSU). In contrast, storms with "Low" inflow (2015-06-02, 2015-07-13, 2020-07-27, 2022-06-06) had little effect on salinity (post-storm salinity > 34.0 PSU), and in the case of 2022-06-06 (34.572 PSU) salinity did not fall below the climatological mean (Table 3). Elevated discharge events were also linked to substantial increases in nutrient concentrations. For example, the 2016-06-20 storm exhibited DIN and $Si(OH)_4$ concentrations of 3.0 µmol L^{-1}, while the 2012-06-22 event, characterized by strong winds and relatively high discharge, yielded DIN concentrations of 1.52 µmol L^{-1}, DIP concentrations of 0.39 µmol L^{-1}, and $Si(OH)_4$ concentrations of 3.136 µmol L^{-1}. Other events also alleviated nutrient limitation, including the 2012-07-12 and 2015-07-13 storms (Table 3). However, due to the relatively low sampling frequency, some storm-related changes in salinity and nutrient concentrations (e.g., from mixing or riverine supply) may not have been captured, as in the cases of 2016-07-02 and 2013-06-15.

https://doi.org/10.5194/egusphere-2025-6235
Preprint. Discussion started: 12 January 2026

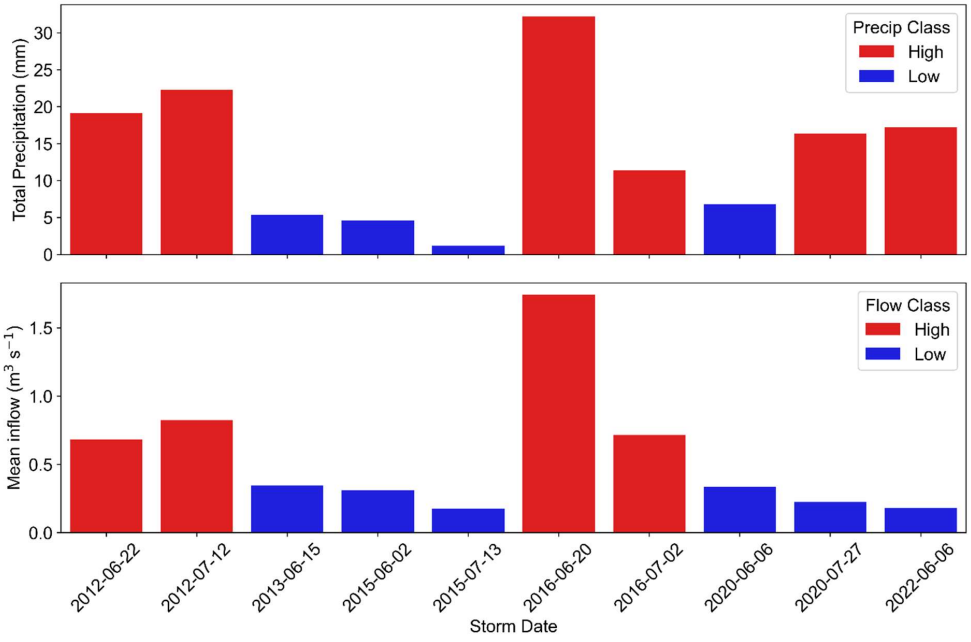

Figure 3. Total precipitation (mm) over ±3 days (a) and mean river inflow ($m^3 s^{-1}$) (b) from the Slack and Wimereux rivers for 10 storms, averaged over ±3 days around each storm. Precipitation classes ("High" and "Low") were defined from June–July rainfall distribution, with the high threshold set at 16.12 mm (80th percentile); inflow classes were defined from June–July river-flow distribution, with the high threshold set at 0.45 $m^3 s^{-1}$ (80th percentile). Blue bars denote "Low" class and red bars denote "High" class in both panels.

Pronounced interannual variability was observed in June–July wind speeds and river inflows (Fig. 4). Years with high inflows (2012, 2013, 2016, 2021) exhibited June–July mean discharge above 0.35 $m^3 s^{-1}$ (Fig. 4) and included storms such as 2012-06-22, 2012-07-12, 2013-06-15, 2016-06-20, and 2016-07-02. In contrast, periods with low monthly inflows (2014, 2015, 2017, June 2018, July 2019, 2020, 2022; Fig. 4) encompassed storms such as 2015-06-02, 2015-07-13, 2020-07-27, and 2022-06-06. Some years were notably windy days (≥10 days per month) despite low inflows, including July 2014, 2015, July 2017, July 2020, and June 2022. June-July months in 2015 and July 2020 all experienced more than 24 windy days above 8 m s^{-1}, coupled with June−July average river flow below 0.35 $m^3 s^{-1}$ (Fig. 4).

Thus, storm impacts arose either from high inflows, from strong winds alone, or from low inflows combined with short windy events (e.g., 2022-06-06). Storms were classified as consecutive when they occurred shortly after a preceding or following storm, such that the effects of the consecutive storms could have persisted. For example, the 2016-07-02 storm followed the 2016-06-20 event, suggesting that storm-driven changes in the marine environment may have been sustained between them. A similar sequence occurred in 2012, when the 2012-07-12 storm followed the 2012-06-22 event.

https://doi.org/10.5194/egusphere-2025-6235
Preprint. Discussion started: 12 January 2026

Table 3. Overview of selected storm events, classified according to maximum precipitation, peak wind intensity, minimum duration, and lowest inflow observed within ±3-day of the storm date. The table also reports the lowest salinity and highest nutrient concentrations recorded during the 14-day post-storm period. Rainiest events were defined as those with total precipitation > 16.12 mm, while windiest events were defined as those in which the third quartile (Q3) of wind stress exceeded 0.1 N m^{-2}. Lowest-flow events were defined as those with discharge < 0.45 $m^3 s^{-1}$.

Date of storm	Most rainy	Most windy	Shortest	Least inflow	Salinity, PSU (Lowest after storm)	Nutrients, µmol L^{-1} (Highest after storm)
2012–06–22	X	X			34.04	DIN (1.523) DIP (0.39) $Si(OH)_4$ (3.136)
2012–07–12	X	X			33.6	DIN (1.517) DIP (0.001) $Si(OH)_4$ (1.056)
2013–06–15		X			33.64	DIN (0.656) DIP (0.096) $Si(OH)_4$ (0.031)
2015–06–02		X		X	34.2	DIN (1.124) DIP (0.079) $Si(OH)_4$ (0.001)
2015–07–13		X		X	34.19	DIN (2.316) DIP (0.342) $Si(OH)_4$ (0.843)
2016–06–20	X		X		33.41	DIN (3.005) DIP (0.091) $Si(OH)_4$ (3.006)
2016–07–02	X	X			33.92	DIN (0.632) DIP (0.091) $Si(OH)_4$ (0.001)
2020–06–06			X		33.959	DIN (0.56) DIP (0.146) $Si(OH)_4$ (1.748)
2020–07–27	X	X		X	34.571	DIN (0.749) DIP (0.089) $Si(OH)_4$ (0.019)
2022–06–06	X		X	X	34.572	DIN (0.732) DIP (0.065) $Si(OH)_4$ (1.65)

https://doi.org/10.5194/egusphere-2025-6235
Preprint. Discussion started: 12 January 2026

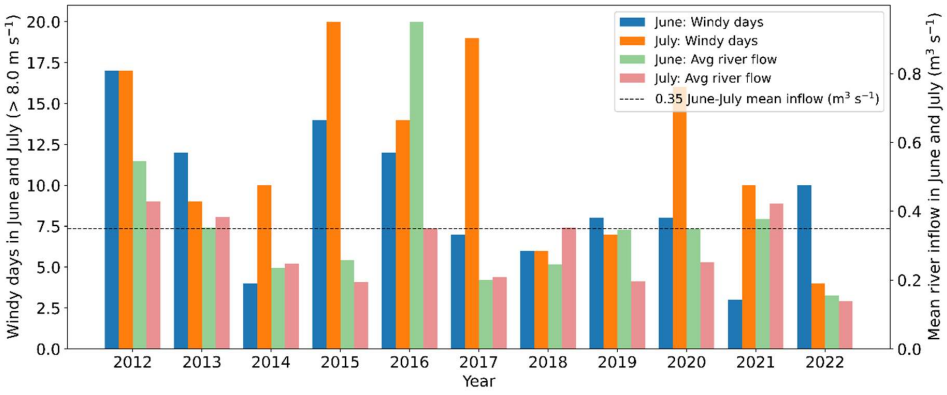

Figure 4. Number of windy days (> 8 m s^{-1}) and average river flow (m^3 s^{-1}) from the Slack and Wimereux rivers during June and July (2012–2022). The dashed line indicates the mean June–July inflow of 0.35 m^3 s^{-1}.

3.2 Exploring summer storm impact on Chl-a and phytoplankton communities

Storms were characterized by the biological response of Chl-a assessed through their pre- and post-storm distributions. Pre-storm mean Chl-a concentrations increased following nearly all storm events, except for those on 2013-06-15 and 2015-07-13 (Fig. 5). In high inflow storms (depicted in green shades, Fig. 5), post-storm increases persisted above the June–July climatological mean of 3.20 µg L^{-1}. The consecutive storm events of 2012 resulted in up to a 4-fold increase in Chl-a concentrations, whereas the consecutive events of 2016 maintained concentrations above the 3.20 µg L^{-1}. A similar persistence of elevated Chl-a was observed following the 2013-06-15 storm, despite the relatively low inflow (depicted in pink shade, Fig. 5) of 0.35 m^3 s^{-1}. A subsequent event on 2013-06-22, with a mean flow rate of 0.39 m^3 s^{-1}, occurred within the 14-day post-storm window and is therefore considered part of the same response as the 2013-06-15 storm. In contrast, low inflow storms (depicted in pink shade, Fig. 5) did not elevate post-storm mean Chl-a concentrations above 3.20 µg L^{-1}. Post-storm responses in Chl-a were more closely aligned with river inflow than with precipitation, as illustrated by the 2020-07-27 and 2022-06-06 storms (Fig. 5; Fig. E1).

The 15-day climatology derived from weekly to biweekly data captured spatial and temporal variations in phytoplankton abundances within each month and revealed that distinct groups characterize different periods of the year (Fig. 6a–f). RedMicro (diatoms and other microphytoplankton) reached abundances on the order of 10^5 cells L^{-1}, increasing from late winter to late spring and declining during summer (Fig. 6a). A sharp increase in RedNano (10^7 cells L^{-1}) from late March to early May reflected the recurring *Phaeocystis globosa* blooms in EEC waters. After spring, RedNano abundances were sustained by nanophytoplankton at ~10^5 cells L^{-1} (Fig. 6b). Other nano-sized groups showed distinct seasonal peaks: HsNano (coccolithophorids) in summer and autumn (Fig. 6c), and OraNano (cryptophytes), which increased steeply from June through autumn, reaching ~10^5 cells L^{-1} (Fig. 6d).

https://doi.org/10.5194/egusphere-2025-6235
Preprint. Discussion started: 12 January 2026

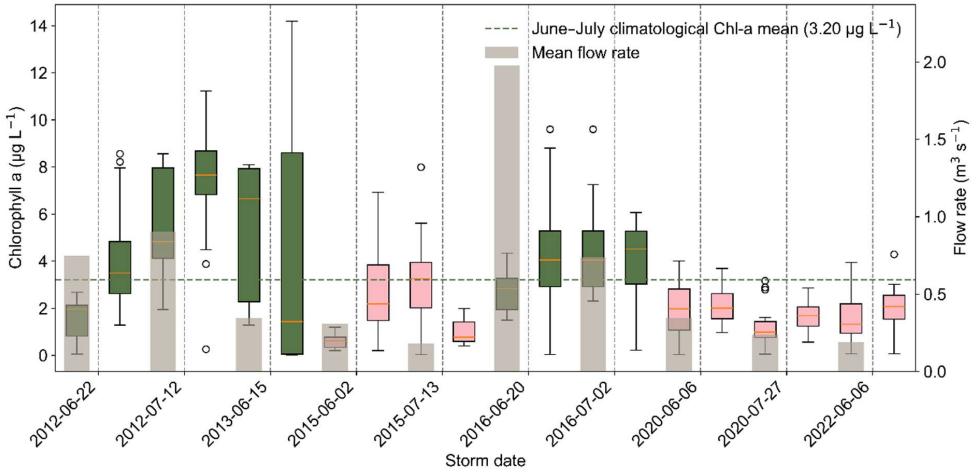

Figure 5. Chlorophyll-a (Chl-a) concentrations before and after the 10 storms, with river inflow (pink bars) and mean inflow (grey bars) overlaid. The green dashed line marks the June–July climatological mean Chl-a concentration (3.20 µg L^{-1}) in the eastern English Channel. Data are compiled from DYPHYRAD, PHYTOBS, and SOMLIT stations. Green and pink shading indicate "High" and "Low" inflow storms, respectively.

During summer, the phytoplankton community was dominated by pico-sized groups, with abundances on the order of 10^7 cells L^{-1} (Fig. 6e–f), including OraPicoProk (*Synechococcus*) and RedPico (picoeukaryotes). The climatology also revealed high standard errors in diatom, pico-sized phytoplankton, and cryptophyte abundances, indicating greater variability during June–July. Spatially, RedMicro were more abundant in coastal waters (Fig. 6a), whereas *Synechococcus* dominated offshore waters (Fig. 6e). Chl-a exhibited similar seasonal and spatial patterns, increasing from late winter to late spring and declining during summer (Fig. C1c). In June and July, *Synechococcus* (OraPicoProk) and picoeukaryotes (RedPico) exhibited the highest mean (8.9×10^6 and 8.4×10^6 cells L^{-1}, respectively), while coccolithophores (HsNano) showed the lowest. Intermediate mean values were observed for nanophytoplankton (1.4×10^6 cells L^{-1}), diatoms (3.4×10^5 cells L^{-1}), and cryptophytes (2.6×10^5 cells L^{-1}) (Fig. 5). An empirical complementary cumulative distribution function (CCDF) was applied to detect shifts in phytoplankton abundances by quantifying the probability of blooms exceeding climatological ranges (Fig. 7A–D). Four storm types were considered. The first type was characterized by high inflow with low wind stress, exemplified by the storm of 2016-06-20, which was the rainiest and had the highest inflow, while showing the least impact of wind (Fig. 2–3). The second type consisted of consecutive storms, with the storm of 2016-07-02 occurring immediately after the previous storm on 2016-06-20. The third type was defined by low inflow with high wind stress, represented by the storm of 2015-07-15, which had the lowest rainfall and inflow but was marked by strong winds (Fig. 2–3). The fourth type involved low inflow with low wind stress, illustrated by the short storm of 2022-06-06, which was classified as high in precipitation yet remained among the lowest in inflow and wind stress. To illustrate changes in community structure across these contrasting storm regimes, see Fig. 7A–D and Table G. The CCDFs of the remaining six storms are presented in the appendix with these storm characterizations (Fig. F1–6).

https://doi.org/10.5194/egusphere-2025-6235
Preprint. Discussion started: 12 January 2026

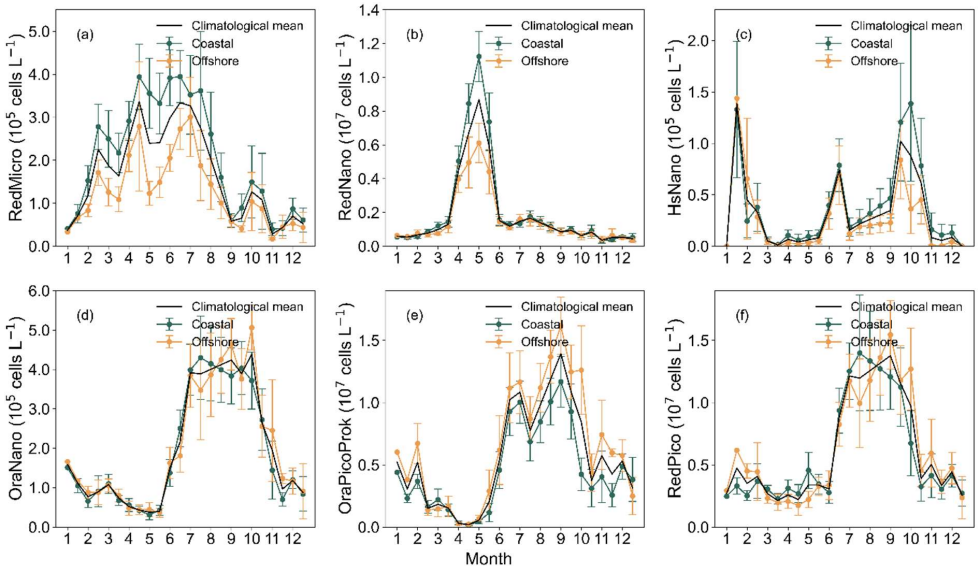

Figure 6. Seasonal and spatial variability of phytoplankton abundances in the eastern English Channel, based on 15-day climatological means from February 2012 to December 2022 estimated from DYPHYRAD data. Mean values (circles) and standard errors (error bars) are shown for coastal (green) and offshore (orange) stations. Subplots (a–f) represent RedMicro (diatoms), RedNano (nanophytoplankton), HsNano (coccolithophorids), OraNano (cryptophytes), OraPicoProk (*Synechococcus*), and RedPico (picoeukaryotes), respectively.

3.2.1 High inflow, low wind stress storm: 2016-06-20

The storm of 20 June 2016 had contrasting impacts across phytoplankton groups and locations. In coastal waters, diatoms responded most strongly, while offshore the dominant signal came from *Synechococcus* (Fig. 7A), mirroring broader summer seasonal patterns (Fig. 6). This event was characterized by high inflow and heavy rainfall, with only short-lived wind stress (Fig. 2), conditions that delivered substantial nutrient inputs to the coast. Across the DYPHYRAD transect, diatom abundances increased significantly from pre- to post-storm (Table G; Anderson–Darling test, $p = 0.001$), with a five-fold rise in the mean (Fig. 7A(a)). At the stations closer to the coast R0–R1, diatom concentrations approached the 90th percentile, and the maximum post-storm abundance was 8.0×10^5 cells L^{-1}. Note that at Point 1–B on 23 June 2016, the diatom *Leptocylindrus danicus* reached 3.0×10^6 cells L^{-1} (Table H1), representing 90% of the diatom assemblage, and was accompanied by a Chl-a concentration of 9.6 µg L^{-1}.

In contrast, nanophytoplankton and cryptophytes declined well below their June–July climatological means (14 and 2.6×10^5 cells L^{-1}, Fig. 6b, 6d respectively), with the sharpest decreases observed at station R0–R1 closer to the coast (Fig. 7A(b–d)). Pico-sized groups, however, showed a different pattern. *Synechococcus* abundances were more than two-fold higher than the climatological mean (8.9×10^6 cells L^{-1}, Fig. 6e), reaching a post-storm mean of 1.6×10^7 cells L^{-1} across the DYPHYRAD transect (Fig. 7A(e)). Offshore stations (R2′, R3, R3′, R4) exhibited the strongest response, with abundances exceeding the 90th percentile and peaking at 2.5×10^7 cells L^{-1}. Picoeukaryotes, by contrast, showed only a slight reduction, maintaining abundances close to their climatological levels (Fig. 7A(f)).

https://doi.org/10.5194/egusphere-2025-6235
Preprint. Discussion started: 12 January 2026

Fig. 7A — High inflow, low wind stress storm: 2016-06-20

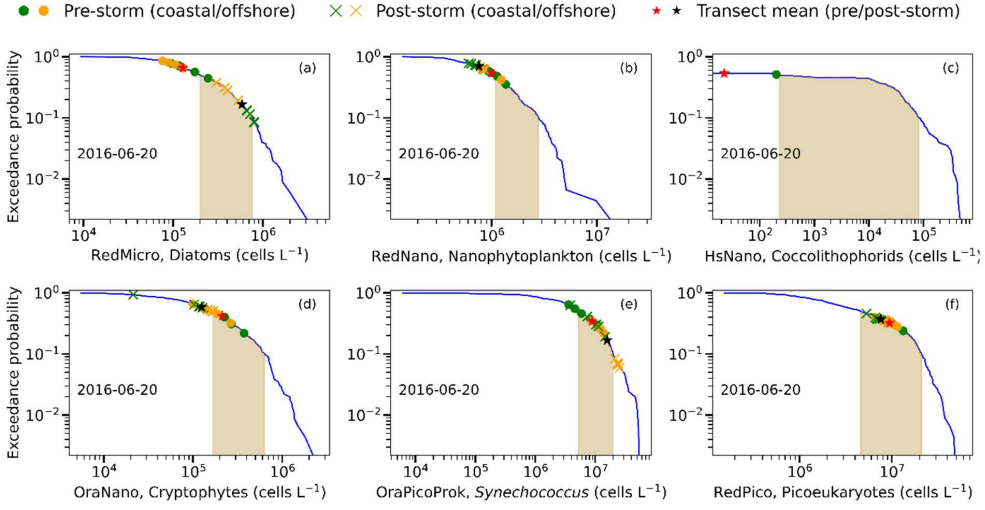

Fig. 7B — Consecutive storm: 2016-07-02 (following 2016-06-20)

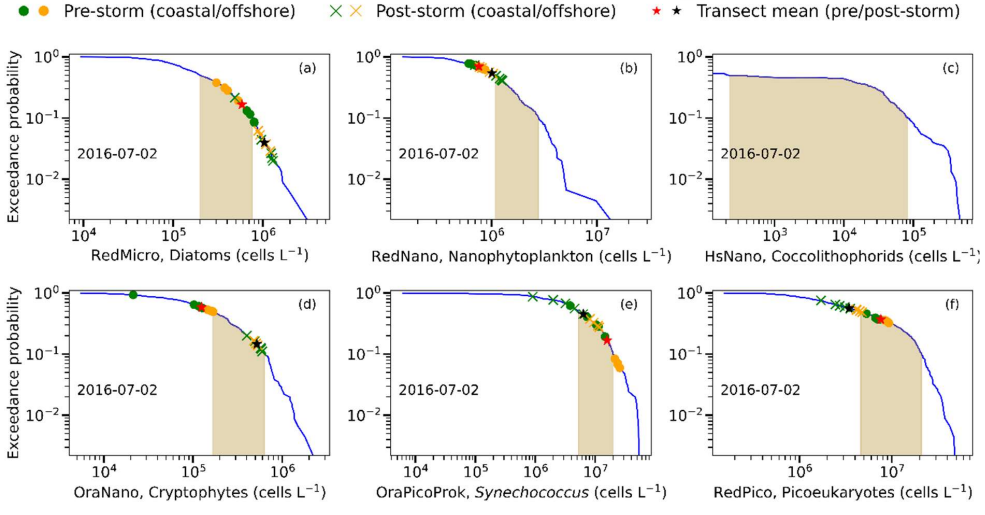

https://doi.org/10.5194/egusphere-2025-6235
Preprint. Discussion started: 12 January 2026

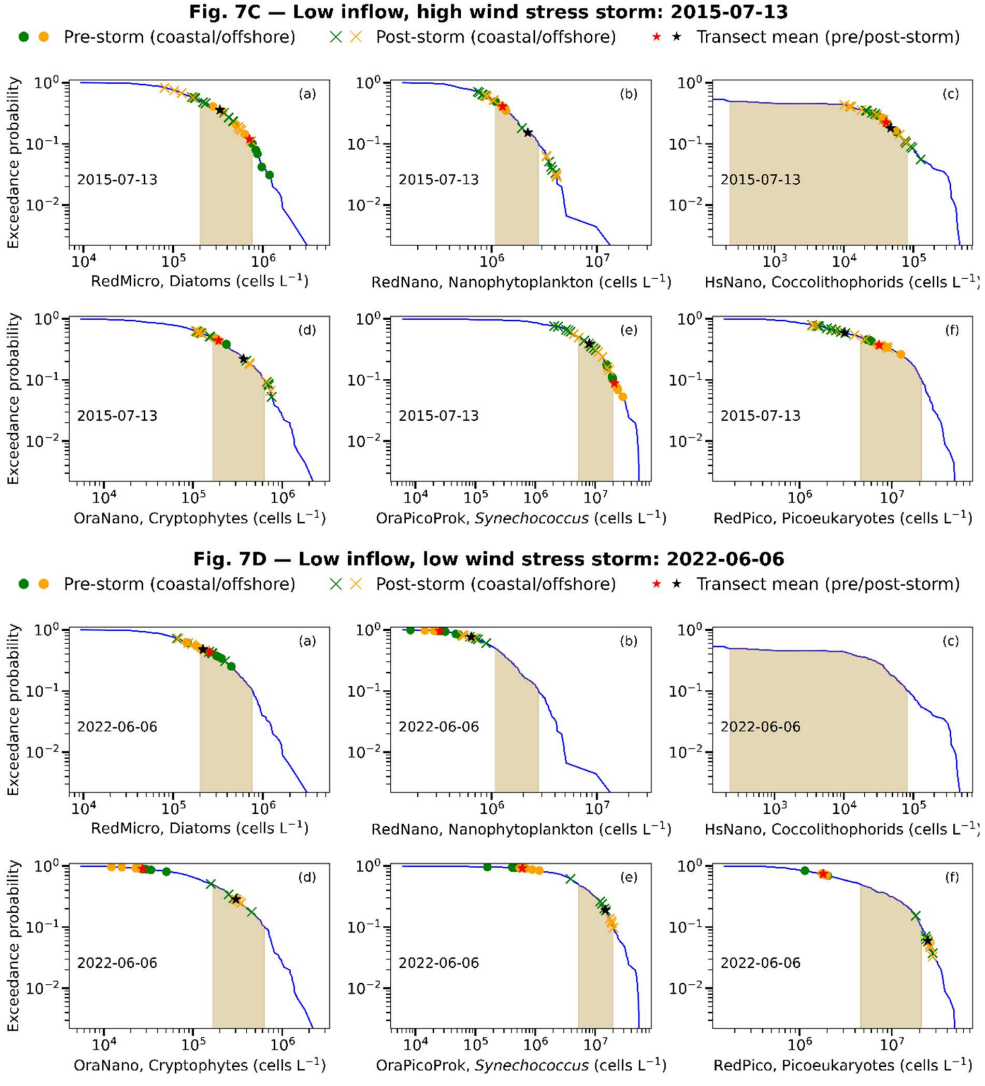

Figure 7. Exceedance probability (CCDF) distributions of six phytoplankton groups along the DYPHYRAD transect during selected storms. Panels show: (A) 2016-06-20, (B) 2016-07-02, (C) 2015-07-13, and (D) 2022-06-06. For each panel: RedMicro (diatoms), RedNano (nanophytoplankton), HsNano (coccolithophorids), OraNano (cryptophytes), OraPicoProk (*Synechococcus*), and RedPico (picoeukaryotes) are shown as subplots (a–f within each panel). Blue lines represent June–July climatological distributions, with shaded areas indicating the 50th–90th percentiles. Pre-storm (−10 days) and post-storm (+14 days) observations are plotted as green (coastal) and orange (offshore) symbols: circles for pre-storm and crosses for post-storm abundances. Red and black stars indicate the transect mean abundances before and after the storm, respectively.

3.2.2 High inflow consecutive storm: 2016-07-02

The 2 July 2016 storm was the windiest event recorded in the analysis (Fig. 2), arriving less than two weeks after the 20 June storm and forming a consecutive high inflow sequence. This back-to-back pattern illustrates how successive storms can reinforce impacts, in this case triggering a pronounced shift toward diatom dominance in the community structure (Fig. 7B). Before the storm, the phytoplankton community was characterized by high abundances of both diatoms and *Synechococcus* (Fig. 7A). Following the storm, diatoms surged dramatically

https://doi.org/10.5194/egusphere-2025-6235
Preprint. Discussion started: 12 January 2026

across the DYPHYRAD transect (Fig. 7B), with post-storm abundances exceeding the 90th percentile (Table G, tail exceedance test, $p < 10^{-7}$; Anderson-Darling test, $p = 0.0013$). Diatom abundances doubled relative to pre-storm levels, reaching a mean of 1.1×10^6 cells L^{-1}, with peaks of 1.3×10^6 cells L^{-1} at coastal stations and 1.2×10^6 cells L^{-1} offshore (Fig. 7B(a)). This bloom marked a shift in dominance from *Leptocylindrus danicus* to *Chaetoceros socialis*. At Point 1-B (Fig. 1), the planktonic diatom *Chaetoceros socialis* reached 1.8×10^6 cells L^{-1} on 4 July 2016 (Table H1), accompanied by a Chl-a concentration of 7.26 µg L^{-1}.

Other groups responded differently. Nanophytoplankton showed only slight increases (Fig. 7B(b)), while cryptophytes rose sharply with a more than a four-fold increase at all stations. (Fig. 7B(d)), with a post-storm mean of 5.2×10^5 cells L^{-1}. At Point L (Fig. 1) on 6 July 2016, cryptophyte abundance peaked at 1.2×10^6 cells L^{-1} (Table H2), indicating a pronounced offshore response. In contrast, *Synechococcus* declined markedly, with post-storm abundances reduced nearly three-fold to a mean of 6.3×10^6 cells L^{-1}, particularly offshore (Fig. 7B(e)).

Picoeukaryotes also decreased, maintaining abundances below pre-storm levels. Both *Synechococcus* and picoeukaryotes declined significantly relative to pre-storm conditions (Table G; AD tests, $p = 0.014$ and $p = 0.001$, respectively), underscoring the contrasting trajectories of pico- and nano-sized groups compared with the strong diatom bloom.

3.2.3 Low inflow, high wind stress storm: 2015-07-13

The 13 July 2015 storm was the windiest event among the low-inflow, low-precipitation storms (Fig. 2). It generated strong turbulence in the water column without delivering additional nutrients from riverine inputs. Under these conditions, the phytoplankton community was reshaped: diatoms and pico-sized groups were suppressed, while nano-sized taxa were favoured (Fig. 7C). Diatom abundances declined sharply in nearshore stations (R0–R2), with the pre-storm mean of 6.8×10^5 cells L^{-1} reduced by 2-fold to 3.3×10^5 cells L^{-1} (Fig. 7C(a)).

In contrast, nano-sized phytoplankton—including nanophytoplankton, coccolithophorids, and cryptophytes—responded positively (Fig. 7C(b–d)). Nanophytoplankton increased significantly relative to pre-storm conditions (Table G; AD test, $p = 0.033$), with post-storm abundances at all stations exceeding the 90th percentile (Table G; tail exceedance test, $p < 0.001$). Their distribution shifted from the 50th to above the 90th percentile (Fig. 7C(b)), with a post-storm mean of 2.2×10^6 cells L^{-1} and a maximum of 4.1×10^6 cells L^{-1}. Coccolithophorids peaked at 1.2×10^5 cells L^{-1} at the R0′ station (Fig. 7C(c)), while cryptophytes showed a strong increase (Fig. 7C(d)) at stations R1–R3 (mean: 3.6×10^5 cells L^{-1}; max: 7.6×10^5 cells L^{-1}), exceeding their climatological mean of 3.0×10^5 cells L^{-1} (Fig. 6).

By contrast, pico-sized groups declined markedly. *Synechococcus* abundances dropped nearly 4-fold, from a pre-storm mean of 2.1 to 8.2×10^6 cells L^{-1}, while picoeukaryotes decreased from 7.4 to 3.2×10^6 cells L^{-1} in the DYPHYRAD transect (Fig. 7C(e–f)). Similarly, at Point L, the suppression was particularly striking: *Synechococcus* fell from 3.4×10^7 cells L^{-1} to 3.6×10^6 cells L^{-1}, and picoeukaryotes from 1.1×10^7 cells L^{-1} to 7.8×10^5 cells L^{-1} by 15 July 2015 (Table H2) with Chl-a concentrations limited to 1.39 µg L^{-1}.

3.2.4 Low inflow, low wind stress storm: 2022-06-06

The 6 June 2022 storm was characterized by both low inflow and low wind stress (Figs. 2, 3), conditions that suggested minimal mixing and limited nutrient supply from rivers. Yet, occurring during a marine heatwave (Simon et al., 2023), this event uniquely reshaped the phytoplankton community. Rather than stimulating diatoms,

https://doi.org/10.5194/egusphere-2025-6235
Preprint. Discussion started: 12 January 2026

the storm amplified pico-sized phytoplankton under the prevailing warm conditions, while diatoms were further suppressed (Fig. 7D).

Diatom abundances declined slightly, with a post-storm mean of 2.0×10^5 cells L^{-1} (Fig. 7D(a)), remaining below the climatological mean of 3.4×10^5 cells L^{-1} (Fig. 6a). Before the storm, populations of nanophytoplankton, cryptophytes, *Synechococcus*, and picoeukaryotes were underdeveloped (Fig. 7D(b–f)). Following the storm, cryptophytes responded modestly at stations R0′, R2′, R3′, and R4, increasing to a post-storm mean of 3.0×10^5 cells L^{-1} (Fig. 7D(d)). In contrast, *Synechococcus* exhibited a dramatic surge at all stations (Fig. 7D(e)), increasing from a post-storm mean of 6.3×10^5 to 1.5×10^7 cells L^{-1}, with an offshore maximum of 2.0×10^7 cells L^{-1}. This increase reflected a significant distributional shift (AD test, $p = 0.001$), though without enrichment of extreme values (Fig. 7D(e)). The strongest response, however, came from picoeukaryotes. They not only shifted significantly (AD test, $p = 0.001$) but also exhibited strong enrichment at all stations except at R0, reaching extreme abundances (Fig. 7D(f)); binomial test, $p < 10^{-7}$; Table G). Post-storm, their mean abundance rose to 2.4×10^7 cells L^{-1}, with maxima of 2.8×10^7 cells L^{-1}.

4 Discussion

Summer storm impacts in the EEC were highly variable between years, arising from different combinations of river inflows and wind events that were in turn modulated by large-scale atmospheric circulation. These patterns directly support our initial hypothesis that different storm types exert distinct ecological impacts. Specifically, our findings confirm that high inflow storms favoured diatoms, wind driven mixing, low inflow summers promoted nanophytoplankton, cryptophytes and pico-sized phytoplankton (Table 4). Nutrient loading through riverine discharge and sediment resuspension can be modulated by precipitation intensity and wind driven mixing, resulting in variable storm impacts on coastal phytoplankton community structure. High inflow storms were predominantly observed in 2012, 2013, 2016, and June 2020, while low inflow windy conditions characterized summer of 2014, 2015, 2017, and July 2020. The 2022 event exemplified a short, low inflow storm with minimal wind duration (<1 h, Table 4). These contrasting phytoplankton dynamics are discussed below.

4.1 Summer storm induced changes in marine environment of the eastern English Channel

In During June–July, south-westerly winds frequently prevail, often exceeding 8 m s^{-1} (Fig. A2, D1). These winds enhance vertical mixing and drive the northward transport of deep and oceanic waters, replenishing nutrients in surface layers (Dulière et al., 2019). In addition, high precipitation events can produce either strong or weak flow rates (Fig. 3). At the same time, south-westerly winds sustain a narrow coastal current, 3–4 km wide, originating from the Bay of Somme and occasionally linked to the Seine estuary (Brylinski et al., 1991). This current is distinct from offshore waters, as reflected in the coastal–offshore salinity gradient, and serves as a conduit for riverine inputs from the Authie, Canche, Slack, Wimereux, and Lianne rivers. Storm impacts are reflected in the coastal water salinity climatology, which exhibits an increasing trend until late May, followed by a decline through the end of July (Fig. C1b). Under south-westerly storm winds (Fig. A2, D1), these surplus inputs can be advected northward into the study area, ultimately reaching the Strait of Dover (Brylinski et al., 1996).

For example, the Somme estuary delivers daily averages of ~500 kmol d^{-1} of silicate and nitrate during June–July (Loquet et al., 2000). Such enrichment from the Bay of Somme has long been associated with the proliferation of diatoms and *Phaeocystis globosa* in the EEC (Brunet et al., 1996).

https://doi.org/10.5194/egusphere-2025-6235
Preprint. Discussion started: 12 January 2026

Table 4. Summary of different storm impacts and their associated physical responses in EEC, highlighting the phytoplankton groups that benefit under each condition. Coastal flow following high inflow storms under south westerly winds transports surplus nutrients from the Somme, Authie and Canche estuaries toward the Strait of Dover along the EEC coast (Brylinski et al., 1991). Wind driven mixing following June–July storms also supplies regenerated nutrients (DIN, DIP) from the degradation of the spring *Phaeocystis* spp. bloom.

Storm type	Storm	Dominant physical mechanism	Physical description	Primary and secondary nutrient source and pathway	Benefiting phytoplankton (size class; taxa)
High Inflow, Low wind stress	2016-06-20 2020-06-06	Horizontal advection	South-westerly wind-driven coastal flow transports river plume northward	Riverine Si, DIN, DIP enriched water advected northward	Diatoms, Pico-sized phytoplankton
		Vertical mixing followed by rapid re-stratification	Brief mixing pulse then quick re-stratification of the water column	Regenerated DIN DIP supply from deep water and sediment	(*Synechococcus* spp. and picoeukaryotes)
High inflow, high wind stress	2012-06-22 2012-07-12 2013-06-15 2016-07-02	Horizontal advection	South-westerly wind-driven coastal flow transports river plume northward	Riverine Si, DIN, DIP enriched water advected northward	Diatoms, Nano-sized phytoplankton
		Vertical Mixing	Turbulent water	Regenerated DIN DIP supply from deep water and sediment resuspension	(Nanophytoplankton, cryptophytes)
Low inflow, high wind stress	2015-06-02 2015-07-13 2020-07-27	Horizontal advection	South-westerly wind-driven coastal flow transports river plume northward	No surplus nutrients from the river to the DYPHYRAD transect	Nano-sized phytoplankton (Nanophytoplankton, cryptophytes)
		Vertical Mixing	Turbulent water	Regenerated DIN DIP supply from deep water and sediment resuspension	
Low inflow, High wind stress (short storm)	2022-06-06	Horizontal advection	South-westerly wind-driven coastal flow transports river plume northward	No surplus nutrients from the river to the DYPHYRAD transect	Pico-sized phytoplankton (*Synechococcus* spp. and picoeukaryotes)
		Vertical mixing followed by rapid re-stratification	Brief mixing pulse then quick re-stratification of the water column	Regenerated DIN DIP supply from deep water and sediment resuspension	

https://doi.org/10.5194/egusphere-2025-6235
Preprint. Discussion started: 12 January 2026

In the English Channel and southern North Sea, summer is often associated with storm activity (Cook et al., 2015; Gronholz et al., 2017; Scholz et al., 2022). Extratropical storms generate extensive cloud cover, rainfall, and riverine inflows, all of which can alter nutrient concentrations, salinity, mixing, and light availability (Jennings et al., 2012; Kasprzak et al., 2017; Rees et al., 2009). The EEC summer months are typically marked by co-limitation of silicate, nitrate, and phosphate (Fig. C1d–f). Despite these constraints, phytoplankton blooms can persist for weeks (e.g., (Rees et al., 2009; Skouroliakou et al., 2022) . For instance, Rees et al. (2009) documented three summer precipitation events that induced freshwater stratification and delivered DIN to surface waters, stimulating primary production. They proposed that storm-driven nutrient loading alleviated DIN limitation, while dissolved organic phosphate was mobilized to meet DIP demand. Such processes may generate synergistic, non-additive responses to dual nutrient enrichments, resulting in enhanced phytoplankton growth (Allgeier et al., 2011).

4.2 Storm impacts on Chl-a and phytoplankton summer communities

Interannual variability in windy days (number of days > 8 m s^{-1}) and inflow during June–July was evident (Fig. 4), with episodes of strong winds in 2015 and 2020, and enhanced riverine discharge in 2012, 2013, 2016, and 2021. Long-term records show that northern Europe has become wetter since the last century (Cook et al., 2015), with alternating wet and dry periods driven by both climate change and natural variability. Corresponding variability was reflected in post-storm Chl-a concentrations (Fig. 5) and phytoplankton community structure (Fig. 7). Since 2012, Chl-a in the DYPHYRAD transect has declined (Hubert et al., 2025a), consistent with earlier observations of interannual shifts in the EEC, including a late-20th-century decrease followed by a rise in the early 2000s (Lefebvre et al., 2011). Similar patterns have been reported elsewhere, with summer primary production responding to rainfall and riverine inputs in the western English Channel (Barnes et al., 2015) and to increased summer winds in the Arctic Ocean (Crawford et al., 2020). These findings suggest that interannual and multidecadal variability in Chl-a may be in part also regulated by distinct storm impacts affecting phytoplankton composition.

Distinct and contrasting patterns emerged between coastal and offshore waters: diatoms were consistently more abundant in coastal zones (Fig. 6a), while *Synechococcus* dominated offshore waters (Fig. 6e). Seasonal dynamics revealed a June–July mean increase in diatom abundance in early July, following the spring bloom (Fig. 6a). *Synechococcus* rose in late May but dipped in early July despite warming temperatures, then recovered by late July as diatoms declined. This crossover suggests that transient meteorological disturbances, including storm-related reductions in light or shifts in nutrient dynamics, temporarily favoured diatoms over *Synechococcus*. The subsequent reversal toward late July reflects a return to more stable summer conditions (Fig 6e). Similarly, high standard errors in diatom, pico-sized phytoplankton, and cryptophyte abundances point to greater fluctuations during June–July (Fig. 6) due to storm driven disturbances.

High inflow storms and diatom (microphytoplankton) responses

In several cases, post-storm increases in Chl-a (Fig. 5) coincided with strong diatom dominance, particularly during the 2012, 2013, and 2016 storm events. These summers were characterized by sustained high diatom concentrations (Hubert et al., 2025), with more than 10 days of winds exceeding 8 m s^{-1} and monthly average river flows above 0.35 m^3 s^{-1} (Fig. 4). Storms create turbulent, nutrient-rich niches that benefit diatoms (Margalef, 1978). Their large cell size allows them to store nutrients during fluctuating nutrient conditions (Litchman et al.,

https://doi.org/10.5194/egusphere-2025-6235
Preprint. Discussion started: 12 January 2026

2009), while their ability to increase Chl-a and other pigments under variable light regimes enhances resilience to rapid changes in irradiance (Kuczynska et al., 2015; Pniewski and Piasecka-Jędrzejak, 2020). High diatom abundances in nearshore waters are therefore expected, given their reliance on riverine inputs such as silicate.

Post-storm peaks in microphytoplankton abundances were often driven by specific diatom taxa such as *Leptocylindrus danicus* and *Chaetoceros socialis*, whose abundances exceeded climatological records by more than 3-fold. *Leptocylindrus danicus* dominated June diatom blooms between 2016 and 2020 (Houliez et al., 2023; Skouroliakou et al., 2022), except in 2018 when *Pseudonitzschia* prevailed, reaching ~10^6 cells L^{-1} and contributing 90% of total diatom abundance at SOMLIT C and PHYTOBS 1-Boulogne stations (Fig. 1). Comparable storm-driven diatom dominance was observed in earlier years. In June–July 2012, consecutive high-inflow storms sustained strong coastal diatom blooms, with mean abundances of 8.4×10^5 cells L^{-1} (Fig. F2a) and post-storm Chl-a concentrations of 7.12 µg L^{-1} (Fig. 5). Following the 19 June 2012 storm, *Leptocylindrus danicus* peaked at 7.6×10^5 cells L^{-1} at Point 1-B (Table H1). Similarly, in June 2013, consecutive storms (15 and 22 June) elevated diatom abundances to maxima of 1.6×10^6 cells L^{-1} (Fig. F3a), with *L. danicus* reaching 5.9×10^6 cells L^{-1} (Table H1) and Chl-a concentrations of 14.19 µg L^{-1} at SOMLIT Point C. Additional evidence of storm-driven responses was observed on 21 July 2016 at SOMLIT Point C near the Lianne River (Fig. 1), following the 11 July storm, when a bloom of *Chaetoceros socialis* reached 3.0×10^6 cells L^{-1} (Table H1). These responses reflect ecological drift, where enhanced growth and reduced competition allow a single taxon to dominate briefly before the community resets (Skouroliakou et al., 2022). The recurrence of these post-storm diatom blooms across multiple years (Table 4; 2012, 2013, 2016–2020) indicates that they are not isolated anomalies but rather a consistent feature of coastal phytoplankton dynamics. High inflow storms in 2012, 2013, 2016, and June 2020 were consistently associated with significant increases in diatom abundances (AD test, $p < 0.05$; Fig. 7A–B, Fig. F3a, F5a), particularly in nearshore waters (R0–R2, Fig. 1), as summarized in Table 4.

Periods of consecutive rainy storms at the end of June may explain the convergence of coastal and offshore diatom climatology in early July (Fig. 6a) (Hubert et al., 2025a; Skouroliakou et al., 2022). In addition, consecutive storms often ensure that this nutrient-rich coastal flow reaches the Strait of Dover, consistent with the high diatom abundances (Fig. 7A–B, F1–3,5) observed in the nearshore and frontal zone R0-R3′. In contrast, the 6 June 2022 storm, characterized by low inflow and weak wind stress (Fig. 7D), did not enhance diatom abundances across the transect. Instead, elevated Chl-a concentrations were detected at Point 1-B and Point C (Table H1; 4.29 and 4.7 µg L^{-1}, respectively), accompanied by a bloom of *Leptocylindrus danicus* (2.27×10^6 cells L^{-1} at Point 1-B). These responses suggest that the impact of low wind stress on coastal flow was largely confined to the south till Boulogne sur mer, while limited inflows from smaller rivers such as the Slack and Wimereux did not enhance diatom growth in the transect (Fig. 7D). Under weak winds, reduced advection creates strong spatial patchiness in the EEC (Bonato et al., 2015). Consequently, it was appropriate that our analysis did not incorporate flow rates from rivers such as the Canche and Liane, as their influence on the transect would have been minimal under these conditions.

High wind stress, low inflow storms and nano-sized phytoplankton responses

June–July periods in 2015 and 2020 have consistently recorded more windy days than high-inflow days, with summer 2015 standing out for its 34 windy days, particularly in July (Fig. 4). Under such conditions, pico- and nano-sized phytoplankton flourished across the EEC (Hubert et al., 2025; Skouroliakou et al., 2022). Summer

https://doi.org/10.5194/egusphere-2025-6235
Preprint. Discussion started: 12 January 2026

stratification of the English Channel (Barnett et al., 2024; Schmitt et al., 2024) provides the backdrop for these dynamics. Wind speeds of ~8 m s^{-1} are sufficient to disrupt stratification (Barnett et al., 2019), mixing the water column and transporting remineralized nutrients from deeper layers to the surface (Table 4) (Williams et al., 2013). Nutrients released from *Phaeocystis globosa* organic matter (Lamy et al., 2009) along the EEC coast can be transported northward by south-westerly winds. Turbulence in the frontal zone (R2–R3′) (Brylinski et al., 1991) explains both the lack of spatial differences in nanophytoplankton climatology (Fig. 6b) and their accumulation in frontal zones (Gieskes et al., 2007; Hubert et al., 2025a), as turbulent conditions favour nutrient consumption. With low inflows limiting silicate supply, diatom growth was constrained, leaving space for nanophytoplankton and cryptophytes to expand by exploiting available DIN and DIP. Windy events illustrate this dynamic clearly. On 2015-07-13 (Fig. 7C), 2015-06-02 (Fig. F4), 2016-07-02 (Fig. 7B), and 2020-07-27 (Fig. F6), pico-sized phytoplankton declined post-storm, replaced by nanophytoplankton. Dry and windy summers such as 2015 and 2020 produced significant increases in nanophytoplankton (Hubert et al., 2025c) (AD test, $p < 0.05$; Fig. 7B, D; Fig. F4b). Metabarcoding analyses have shown that pico- and nano-sized phytoplankton communities were composed of the *Synechococcus*, coccolithophorid *Emiliania* and the nanoplanktonic diatom *Minidiscus*, while cryptophyte peaks — dominated by *Plagioselmis* — were observed in July 2016, 2018, and 2020 (Skouroliakou et al., 2022).

Low wind stress storms and pico-sized phytoplankton responses

By contrast, the 2022-06-06 storm produced a different outcome. With only a brief one-hour windy period, the post-storm community was dominated by pico-sized phytoplankton (Table 4), with only marginal increases in nanophytoplankton (Fig. 7D). This event unfolded during concurrent marine and atmospheric heatwaves (Guinaldo et al., 2023; Simon et al., 2023), which elevated sea surface temperatures and reduced cloud cover and wind speeds, creating favourable conditions for pico-sized taxa. Their high surface-to-volume ratio confers a competitive advantage under oligotrophic conditions, enabling efficient nutrient uptake even when concentrations are low (Raven, 1984). The EEC remained stratified until 19 June 2022, when a short four-hour windy event occurred (not shown here). By late June, *Synechococcus* and picoeukaryotes reached exceptional abundances offshore (1.0×10^8 and 2.3×10^8 cells L^{-1} at Point L) and at the coast (4.8×10^7 and 1.8×10^7 cells L^{-1} at Point C; Table H2). Similar low-wind storms in June 2016 (Fig. 7A) and 2020 (Fig. F5) also favoured pico-sized phytoplankton. Low wind stress storms (e.g., 2020-06-06 and 2022-06-06) were associated with significant increases in pico-sized phytoplankton (AD test, $p < 0.05$) and not a significant decrease (e.g., 2016-06-20). Overall, pico- and nano-sized phytoplankton are well adapted to low nutrient concentrations, efficiently acquiring resources and sustaining growth under windy, low-inflow conditions. Wind-driven mixing maintains sufficient nutrient levels in surface waters without fully replenishing them, favouring pico-sized taxa during most summers (Fig. 6e–f; Hubert et al., 2025a).

5 Concluding remarks

The higher frequency and intensity of storms in recent years (Wasko et al., 2021) causes increasing disturbances to the water column by changing turbidity, salinity and nutrients. The present study revealed that summer phytoplankton dynamics were strongly shaped by the interplay of stratification, turbulence, and riverine inputs due to storms. Summer storm impacts in the EEC were highly variable between years, arising from different

https://doi.org/10.5194/egusphere-2025-6235
Preprint. Discussion started: 12 January 2026

combinations of river inflows and wind storms that are themselves modulated by large-scale atmospheric circulation. Storms repeatedly disrupted seasonal succession, generating short-lived but pronounced shifts in community structure, including transient monospecific peaks. Such disturbance-driven variability aligns with the broader understanding that biological responses under fluctuating conditions can be governed by stochastic processes such as ecological drift and dispersal (Jurburg et al., 2017). Although we did not explicitly quantify stochasticity in this study, our results suggest that storms acted as environmental disturbances capable of supporting stochastic phytoplankton growth, consistent with the finding that stochastic processes explained 69% of summer community turnover in the EEC (Skouroliakou et al., 2022). Such disturbance-driven conditions may facilitate the emergence of unpredictable blooms, including monospecific events such as *Leptocylindrus danicus*. Similar storm-related shifts have been documented in other aquatic systems—for example, the post-storm dominance of cryptomonads in a temperate lake (Jacobsen and Simonsen, 1993) and reduced phytoplankton diversity linked to stochastic processes in the Yangtze River estuary (Xian et al., 2024)—highlighting the wider relevance of our observations i.e., post-storm high abundance of certain phytoplankton groups. Finally, our study highlighted how disturbances such as storms act as environmental drivers that foster stochastic growth, a mechanism that should be considered into models to better predict ecosystem responses under increasing frequency of extreme events.

Appendix A: Wind speed and direction during storms

The wind speed and direction during the 10 storms is shown in Fig. A1–A2 respectively. The dataset consists of hourly wind measurements, which capture the high variability in wind speed. The longest storm occurred on 2016-07-02, when wind speeds never dropped below 8 m s^{-1} during the ±3-day period around the peak. In contrast, the shortest storms were on 2016-06-20 and 2022-06-06, when extreme wind speeds (≥11.3 m s^{-1}) lasted for no more than 1 hour within the ±3-day window. As mentioned previously, the ±3-day period was used to calculate wind stress (Fig. 2) at the sea surface. Across all events, the strongest winds during the ±3-day periods were consistently directed from the south-west. Unfortunately, subsurface current data are not available, preventing us from showing the corresponding direction of the coastal flow.

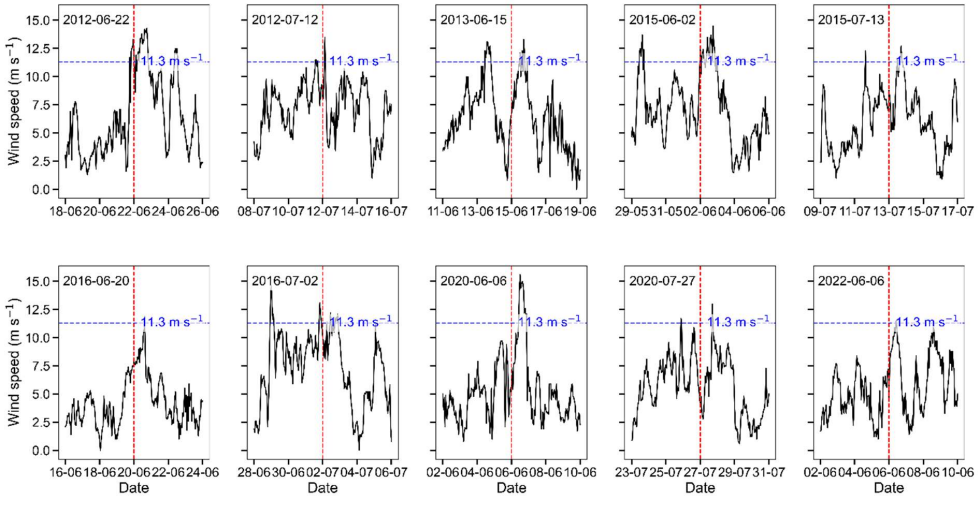

https://doi.org/10.5194/egusphere-2025-6235
Preprint. Discussion started: 12 January 2026

Figure A1. Wind speed time series during storm events (±4 days). The red dashed line indicates the selected central storm day, with analyses conducted over a ±3-day window around this reference point.

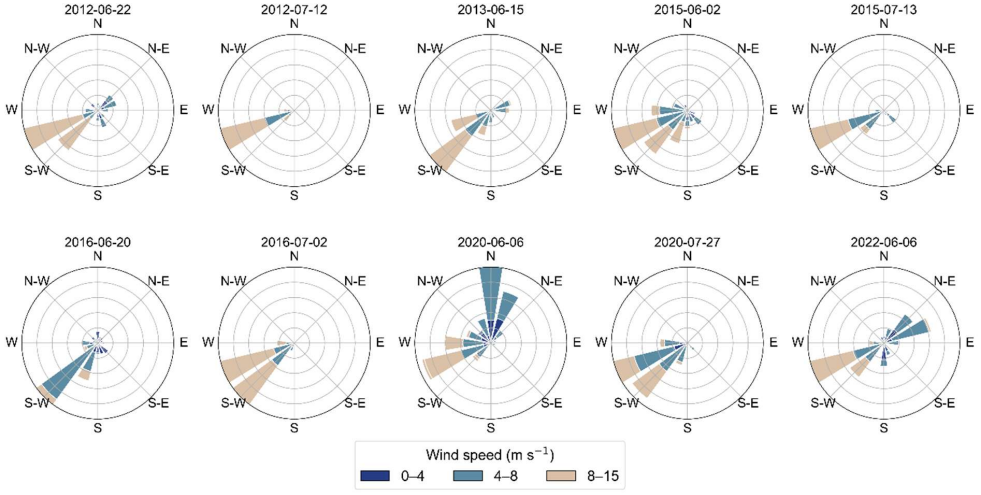

Figure A2. Wind direction and speed during storm events (±3-day) at the Boulogne-Sur-Mer meteorological station. Polar plots show the frequency of winds by compass sector, with colours indicating wind speed categories.

Appendix B: Frequency distributions of June–July precipitation and river inflow

Frequency distributions of June–July precipitation and river inflow were visualized using bar plots of storm totals and means within ±3 days of identified storm dates (Fig. B1). The 80th percentile of these aggregates was used to classify storm intensity: 16.12 mm for precipitation and 0.45 $m^3 s^{-1}$ for river inflow. Storm periods were then categorized as "High" or "Low" relative to these thresholds, and precipitation totals and mean inflows were compared against them to assess storm intensity (Fig. 3).

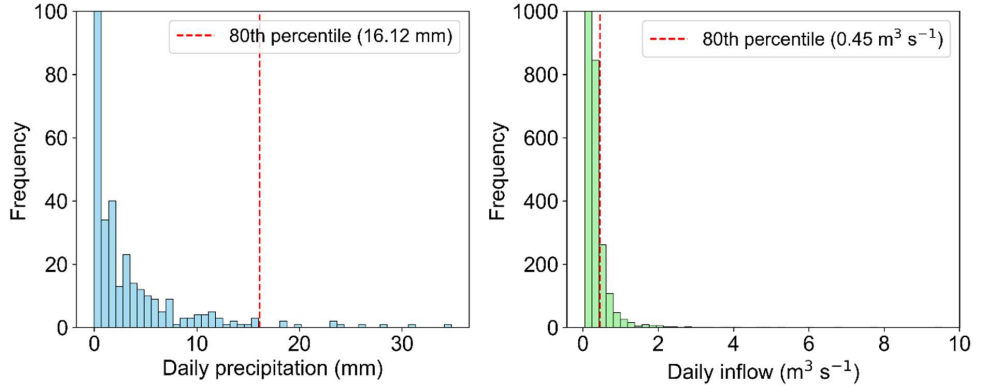

Figure B1. Frequency distributions of June–July precipitation (left) and river inflow (right) at the study site. Red dashed lines indicate the 80th percentile thresholds, calculated from normalized ±3-day total precipitation and mean inflow values. These thresholds were used to identify storm impacts as 'High' or 'Low' classes precipitation and river discharge.

https://doi.org/10.5194/egusphere-2025-6235
Preprint. Discussion started: 12 January 2026

Appendix C: Seasonal and spatial variability of environmental variables

Seasonal and spatial variability indicates that nearshore stations (R0–R2) are more strongly affected by seasonal progression, particularly reflected in salinity (Fig. C1b) and chlorophyll-a (Fig. C1c). Spatial difference in salinity and Chl-a suggests that EEC waters are strongly influenced by riverine inputs along the coast. Two peaks are observed during spring: the first dominated by diatoms, and the second in April by *Phaeocystis globosa*. A third chlorophyll-a peak occurs in June–July, followed by a fourth, smaller peak in autumn. Even though nutrient limitation was strongest in June and July, Chl-a levels were nevertheless sustained during this period.

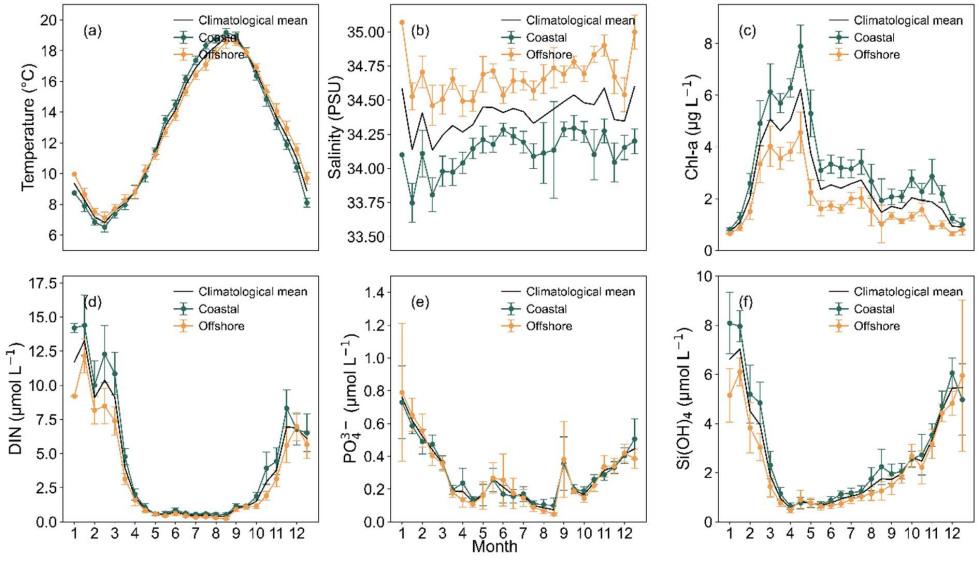

Figure C1. Seasonal and spatial variability of environmental variables; panels show: (a) sea surface temperature (°C), (b) salinity (PSU), (c) chlorophyll-a (μg L^{-1}), (d) dissolved inorganic nitrogen (DIN, μmol L^{-1}), (e) dissolved inorganic phosphorus (DIP, μmol L^{-1}), and (f) dissolved inorganic silicate (DISi, μmol L^{-1}). Data are based on 15-day climatological means from February 2012 to December 2022 using observations from DYPHYRAD, SNO SOMLIT, and SNO Phytobs. Mean values (circles) and standard errors of the mean (SEM; error bars) are shown for coastal (green) and offshore (orange) stations.

Appendix D: Climatology of wind speed and direction

Figure D1 shows the climatology of wind speed and direction across the year. During spring, wind direction is predominantly north-easterly, whereas from June onward it is dominated by south-westerly winds for the remainder of the year.

https://doi.org/10.5194/egusphere-2025-6235
Preprint. Discussion started: 12 January 2026

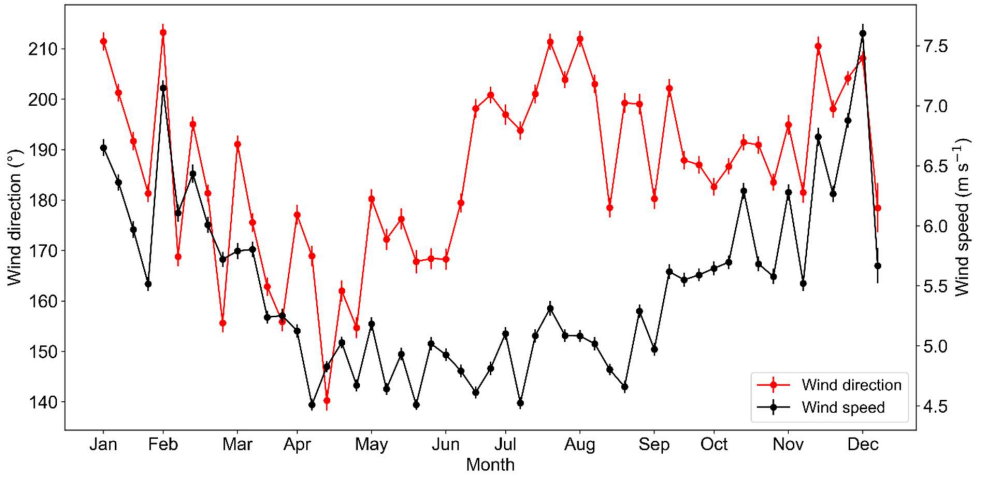

Figure D1. Monthly climatology of wind speed (black line, mean ± SEM) and wind direction (red line, mean ± SEM) at the study site. The June–July period is characterized by a clear predominance of south-westerly winds, coinciding with the summer storm season.

Appendix E: Variability of Chl-a concentrations in relation to storms and precipitation

Figure E1 shows the pre- and post-storm distributions relative to precipitation occurring within ±3 days. Precipitation and post-storm chlorophyll-a did not exhibit a linear relationship across storms.

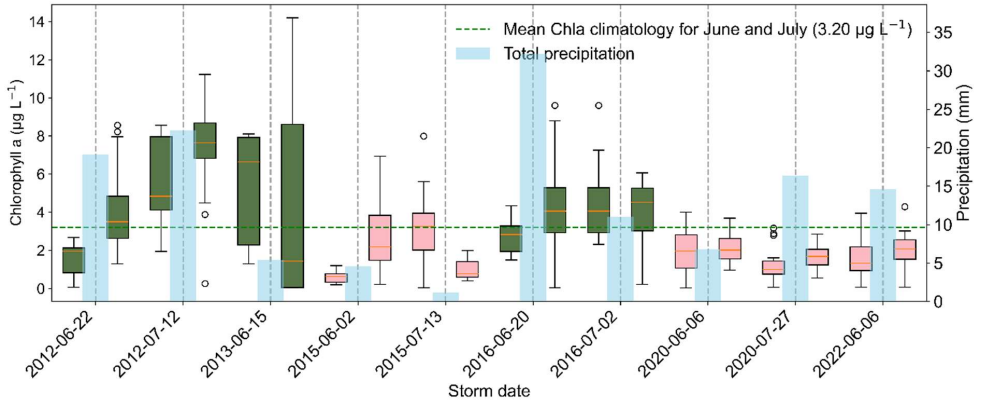

Figure E1. Chlorophyll a (Chl-a) concentrations before and after 10 storm events, overlaid by total precipitation (blue bar). The green dashed line marks the June–July climatological mean Chl-a (3.20 µg L^{-1}). Green and pink shading indicate the "High" and "Low" inflow storms, respectively.

Appendix F: Phytoplankton CCDFs during the storm events

The CCDFs of the remaining six storms are shown in Fig. F1–F6. Storms on 2012-06-22, 2012-07-12, and 2013-06-15 were characterized by high inflow and high wind stress, with post-storm distributions dominated by diatoms. In the latter two storms, elevated diatom abundances persisted until mid-July, replacing nanophytoplankton (Fig. F2–3). The storm of 2015-06-02 was marked by low inflow but high wind stress in early June, supporting a nanophytoplankton bloom that was subsequently overtaken by high abundances of *Phaeocystis globosa* (Fig.

https://doi.org/10.5194/egusphere-2025-6235
Preprint. Discussion started: 12 January 2026

F4(b)). The storm of 2020-06-06 received additional precipitation and inflow on 2020-06-16 (not shown here), supporting diatoms and pico-sized phytoplankton (Fig. F5) under low wind stress (Fig. 2). Finally, the storm of 2020-07-27, characterized by high wind stress and low inflow, resulted in increased nanophytoplankton and replacement of picoeukaryotes in nearshore waters (Fig. F6).

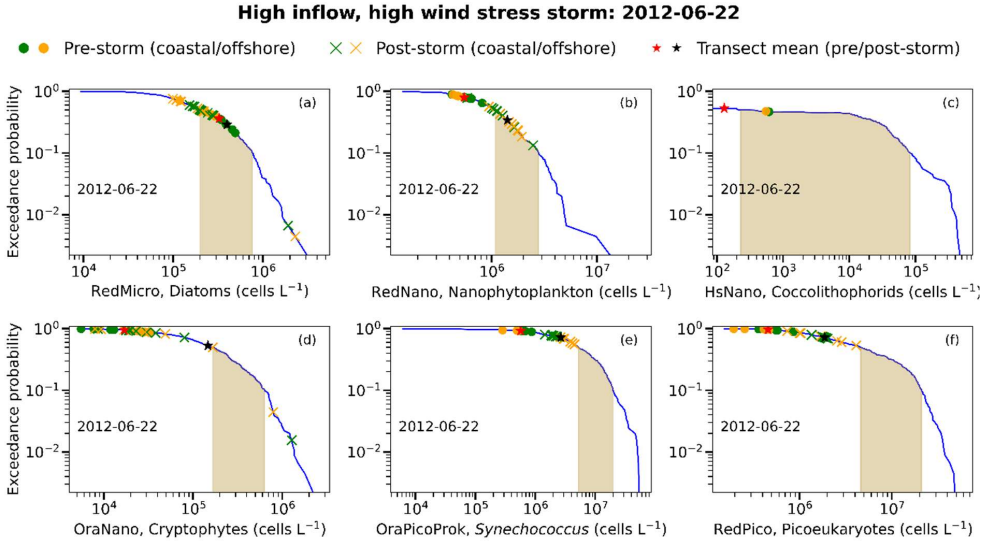

Figure F1. Exceedance probability (CCDF) distributions of six phytoplankton groups along the DYPHYRAD transect during the storm of 2012-06-22. For each panel, RedMicro (diatoms), RedNano (nanophytoplankton), HsNano (coccolithophorids), OraNano (cryptophytes), OraPicoProk (*Synechococcus*), and RedPico (picoeukaryotes) are shown as subplots (a–f). Blue lines represent June–July climatological distributions, with shaded areas indicating the 50th–90th percentiles. Pre-storm (−10 days) and post-storm (+14 days) observations are shown as green (coastal) and orange (offshore) symbols, with circles indicating pre-storm and crosses indicating post-storm abundances. Red and black stars indicate transect-mean abundances before and after the storm, respectively.

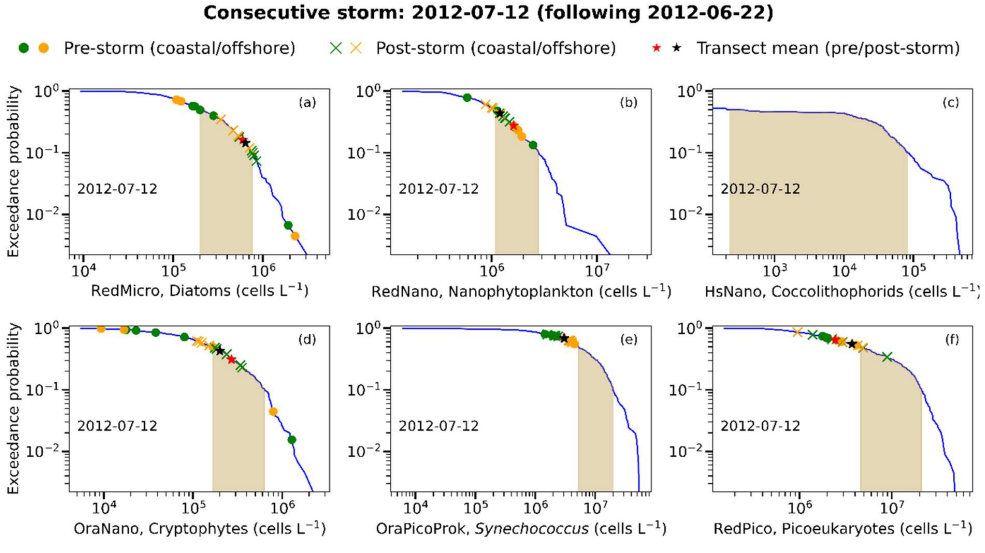

Figure F2. Exceedance probability (CCDF) distributions of six phytoplankton groups along the DYPHYRAD transect during the storm of 2012-07-12. For each panel, RedMicro (diatoms), RedNano (nanophytoplankton), HsNano (coccolithophorids),

https://doi.org/10.5194/egusphere-2025-6235
Preprint. Discussion started: 12 January 2026

OraNano (cryptophytes), OraPicoProk (*Synechococcus*), and RedPico (picoeukaryotes) are shown as subplots (a–f). Blue lines represent June–July climatological distributions, with shaded areas indicating the 50th–90th percentiles. Pre-storm (−10 days) and post-storm (+14 days) observations are shown as green (coastal) and orange (offshore) symbols, with circles indicating pre-storm and crosses indicating post-storm abundances. Red and black stars indicate transect-mean abundances before and after the storm, respectively.

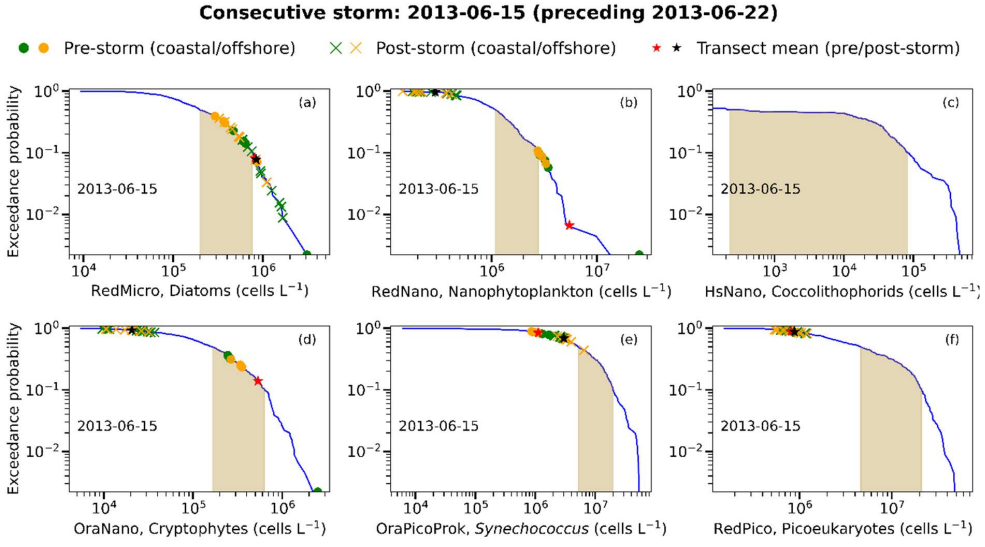

Figure F3. Exceedance probability (CCDF) distributions of six phytoplankton groups along the DYPHYRAD transect during the storm of 2013-06-15. For each panel, RedMicro (diatoms), RedNano (nanophytoplankton), HsNano (coccolithophorids), OraNano (cryptophytes), OraPicoProk (*Synechococcus*), and RedPico (picoeukaryotes) are shown as subplots (a–f). Blue lines represent June–July climatological distributions, with shaded areas indicating the 50th–90th percentiles. Pre-storm (−10 days) and post-storm (+14 days) observations are shown as green (coastal) and orange (offshore) symbols, with circles indicating pre-storm and crosses indicating post-storm abundances. Red and black stars indicate transect-mean abundances before and after the storm, respectively.

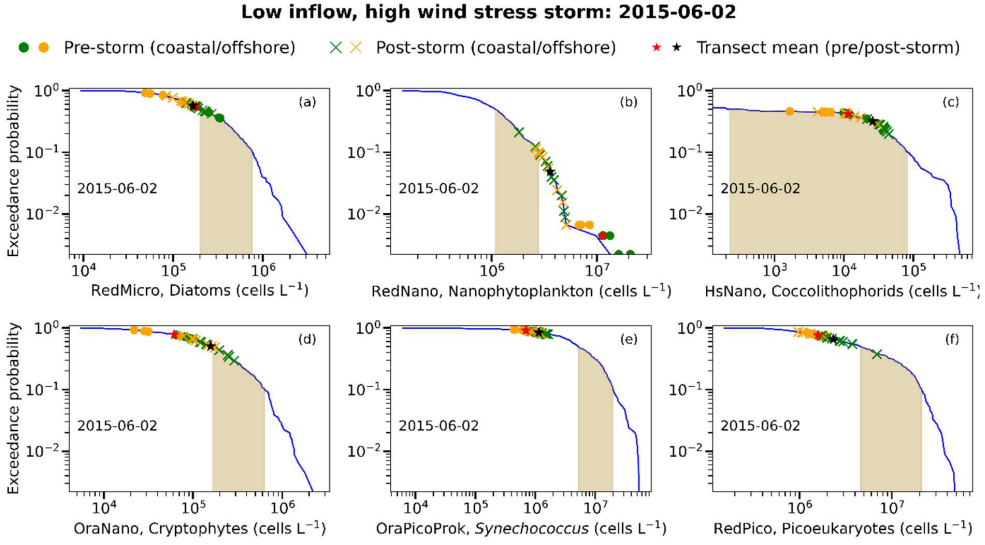

Figure F4. Exceedance probability (CCDF) distributions of six phytoplankton groups along the DYPHYRAD transect during the storm of 2015-06-02. For each panel, RedMicro (diatoms), RedNano (nanophytoplankton), HsNano (coccolithophorids), OraNano (cryptophytes), OraPicoProk (*Synechococcus*), and RedPico (picoeukaryotes) are shown as subplots (a–f). Blue lines

https://doi.org/10.5194/egusphere-2025-6235
Preprint. Discussion started: 12 January 2026

represent June–July climatological distributions, with shaded areas indicating the 50th–90th percentiles. Pre-storm (−10 days) and post-storm (+14 days) observations are shown as green (coastal) and orange (offshore) symbols, with circles indicating pre-storm and crosses indicating post-storm abundances. Red and black stars indicate transect-mean abundances before and after the storm, respectively.

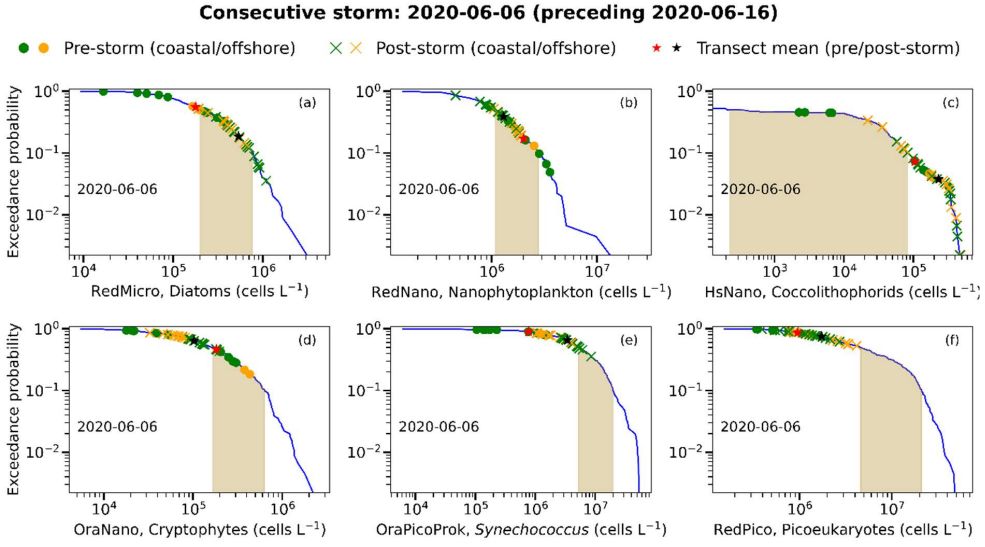

Figure F5. Exceedance probability (CCDF) distributions of six phytoplankton groups along the DYPHYRAD transect during the storm of 2020-06-06. For each panel, RedMicro (diatoms), RedNano (nanophytoplankton), HsNano (coccolithophorids), OraNano (cryptophytes), OraPicoProk (*Synechococcus*), and RedPico (picoeukaryotes) are shown as subplots (a–f). Blue lines represent June–July climatological distributions, with shaded areas indicating the 50th–90th percentiles. Pre-storm (−10 days) and post-storm (+14 days) observations are shown as green (coastal) and orange (offshore) symbols, with circles indicating pre-storm and crosses indicating post-storm abundances. Red and black stars indicate transect-mean abundances before and after the storm, respectively.

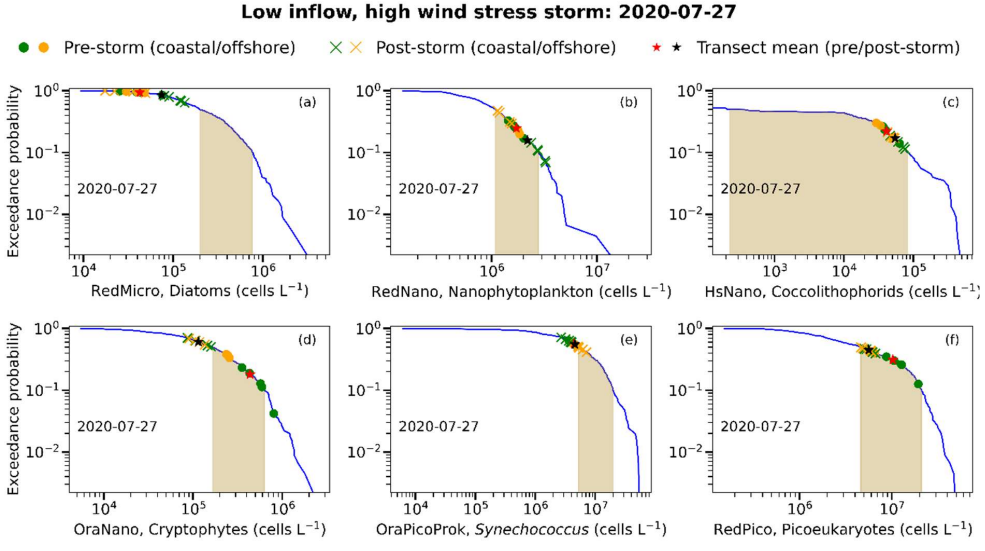

Figure F6. Exceedance probability (CCDF) distributions of six phytoplankton groups along the DYPHYRAD transect during the storm of 2020-07-27. For each panel, RedMicro (diatoms), RedNano (nanophytoplankton), HsNano (coccolithophorids), OraNano (cryptophytes), OraPicoProk (*Synechococcus*), and RedPico (picoeukaryotes) are shown as subplots (a–f). Blue lines represent June–July climatological distributions, with shaded areas indicating the 50th–90th percentiles. Pre-storm (−10 days)

https://doi.org/10.5194/egusphere-2025-6235
Preprint. Discussion started: 12 January 2026

and post-storm (+14 days) observations are shown as green (coastal) and orange (offshore) symbols, with circles indicating pre-storm and crosses indicating post-storm abundances. Red and black stars indicate transect-mean abundances before and after the storm, respectively.

Appendix G: Abundance responses to storms: Anderson-Darling and Exceedance test results

Table G1. Results of distribution-wide (Anderson-Darling) and tail-focused exceedance tests used to characterize phytoplankton responses to storm events in the eastern English Channel. The Anderson-Darling test detects overall shifts in abundance distributions between pre- and post-storm samples, while the binomial exceedance test evaluates whether the frequency of extreme post-storm abundances (above the 90th percentile climatology) differs significantly from expectation (i.e., 90th percentile). Significant *p*-values ($p < 0.05$) indicate either a distributional shift or enrichment of extreme values.

Storm date	Phytoplankton group	Pre-storm samples (n)	Post-storm samples (n)	Anderson-Darling (AD) statistic	AD *p*-value	Tail exceedance test *p*-value
2012-06-22	RedMicro	9	18	3.25	0.015	0.55
	RedNano	9	18	11.28	0.001	1
	HsNano	9	18			1
	OraNano	9	18	1.76	0.060	0.55
	OraPicoProk	9	18	12.47	0.001	1
	RedPico	9	18	12.04	0.001	1
2012-07-12	RedMicro	9	9	3.77	0.01	0.05
	RedNano	9	9	3.76	0.01	1
	HsNano	9	9			1
	OraNano	9	9	2.45	0.03	1
	OraPicoProk	9	9	-0.30	0.25	1
	RedPico	9	9	1.67	0.06	1
2013-06-15	RedMicro	9	18	-0.003	0.25	0.0001
	RedNano	9	18	12.47	0.001	1
	HsNano	9	18			1
	OraNano	9	18	12.47	0.001	1
	OraPicoProk	9	18	12.47	0.001	1
	RedPico	9	18	0.85	0.14	1
2015-06-02	RedMicro	9	18	1.43	0.08	1
	RedNano	9	18	12.47	0.001	7.85×10^{-13}
	HsNano	9	18	3.99	0.008	1
	OraNano	9	18	11.25	0.001	1
	OraPicoProk	9	18	8.37	0.001	1

https://doi.org/10.5194/egusphere-2025-6235
Preprint. Discussion started: 12 January 2026

	RedPico	9	18	1.00	0.12	1
2015-07-13	RedMicro	9	18	5.84	0.001	1
	RedNano	9	18	2.40	0.03	0.0001
	HsNano	9	18	1.75	0.06	0.27
	OraNano	9	18	2.41	0.03	0.006
	OraPicoProk	9	18	10.90	0.001	1
	RedPico	9	18	7.77	0.001	1
2016-06-20	RedMicro	9	9	8.83	0.001	0.23
	RedNano	9	9	3.95	0.008	1
	HsNano	9	9			1
	OraNano	9	9	2.77	0.02	1
	OraPicoProk	9	9	1.41	0.08	0.008
	RedPico	9	9	1.37	0.08	1
2016-07-02	RedMicro	9	9	6.19	0.001	9.41×10^{-8}
	RedNano	9	9	2.74	0.02	1
	HsNano	9	9			1
	OraNano	9	9	8.83	0.001	1
	OraPicoProk	9	9	3.36	0.01	1
	RedPico	9	9	8.83	0.001	1
2020-06-06	RedMicro	12	27	12.18	0.001	0.13
	RedNano	12	27	4.21	0.006	1
	HsNano	12	27	3.95	0.008	6.1×10^{-15}
	OraNano	12	27	5.18	0.002	1
	OraPicoProk	12	27	13.70	0.001	1
	RedPico	12	27	3.14	0.01	1
2020-07-27	RedMicro	8	9	1.51	0.07	1
	RedNano	8	9	1.00	0.12	0.23
	HsNano	8	9	3.64	0.01	1
	OraNano	8	9	8.30	0.001	1
	OraPicoProk	8	9	1.07	0.11	1

https://doi.org/10.5194/egusphere-2025-6235
Preprint. Discussion started: 12 January 2026

	RedPico	8	9	4.43	0.005	1
2022-06-06	RedMicro	9	9	-0.50	0.25	1
2022-06-06	RedNano	9	9	8.83	0.001	1
2022-06-06	HsNano	9	9			1
2022-06-06	OraNano	9	9	8.83	0.001	1
2022-06-06	OraPicoProk	9	9	8.83	0.001	0.61
2022-06-06	RedPico	9	9	8.83	0.001	9.4×10^{-8}

Appendix H: Phytoplankton taxa and functional group observations

695 **Table H1.** Dominant phytoplankton taxa identified in the EEC between 20 May and 10 August during storm years (2012, 2013, 2015, 2016, 2020, 2022). For each sampling date, the phytoplankton taxa with the highest cell abundance (cells L^{-1}) were selected from PHYTOBS observations at the Point-1B and Wimereux SOMLIT-C stations.

Dataset	Date	Long. (° E)	Lat. (° N)	Phytoplankton taxa	Abundance (Cells L^{-1})	Chl-a (µg L^{-1})
Point 1 Boulogne	2012–05–24	1.548	50.753	*Guinardia delicatula*	2.7×10^5	7.34
Point 1 Boulogne	2012–06–05	1.548	50.753	*Leptocylindrus danicus*	3.9×10^5	3.32
Point 1 Boulogne	2012–06–19	1.548	50.753	*Leptocylindrus danicus*	7.6×10^5	2.22
Point 1 Boulogne	2012–07–25	1.548	50.753	*Leptocylindrus danicus*	2.4×10^5	11.23
Point 1 Boulogne	2013–05–30	1.548	50.753	*Phaeocystis*	4.2×10^5	4.04
Point 1 Boulogne	2013–06–20	1.548	50.753	*Leptocylindrus danicus*	2.8×10^6	9.86
Point 1 Boulogne	2013–06–26	1.548	50.753	*Leptocylindrus danicus*	3.0×10^6	12.96
Point 1 Boulogne	2013–07–23	1.548	50.753	*Cryptophyceae*	1.0×10^5	2.53
Point 1 Boulogne	2013–08–05	1.548	50.753	*Rhizosolenia imbricata + styliformis*	3.7×10^5	3.8
Point 1 Boulogne	2015–06–15	1.548	50.753	*Leptocylindrus danicus*	8.4×10^4	3.61
Point 1 Boulogne	2015–06–26	1.548	50.753	*Leptocylindrus danicus*	2.6×10^6	7.71
Point 1 Boulogne	2015–07–16	1.548	50.753	*Cryptophyceae*	3.1×10^4	1.39
Point 1 Boulogne	2016–05–24	1.548	50.753	*Phaeocystis*	2.7×10^6	1.94
Point 1 Boulogne	2016–06–08	1.548	50.753	*Phaeocystis*	4.8×10^5	1.57
Point 1 Boulogne	2016–06–23	1.548	50.753	*Leptocylindrus danicus*	3.1×10^6	9.6

https://doi.org/10.5194/egusphere-2025-6235
Preprint. Discussion started: 12 January 2026

Point 1 Boulogne	2016–07–04	1.548	50.753	*Chaetoceros socialis + socialis f. radians*	1.8×10^6	7.26
Point 1 Boulogne	2016–07–18	1.548	50.753	*Chaetoceros socialis f. radians*	1.0×10^6	8.75
Point 1 Boulogne	2020–05–26	1.548	50.753	*Gymnodiniales*	7.5×10^4	1.65
Point 1 Boulogne	2020–06–09	1.548	50.753	*Cryptophyceae*	4.9×10^4	2.66
Point 1 Boulogne	2020–06–24	1.548	50.753	*Cryptophyceae*	4.2×10^4	4.14
Point 1 Boulogne	2020–07–10	1.548	50.753	*Chaetoceros socialis f. radians*	5.4×10^4	1.34
Point 1 Boulogne	2020–07–20	1.548	50.753	*Chaetoceros socialis + socialis f. radians*	1.4×10^6	2.88
Point 1 Boulogne	2020–08–04	1.548	50.753	*Rhizosolenia imbricata + styliformis*	3.7×10^4	1.55
Point 1 Boulogne	2022–06–01	1.548	50.753	*Chaetoceros socialis + socialis f. radians*	2.4×10^5	4.59
Point 1 Boulogne	2022–06–14	1.548	50.753	*Chaetoceros socialis + socialis f. radians*	2.2×10^6	4.7
Point 1 Boulogne	2022–06–27	1.548	50.753	*Chaetoceros socialis + socialis f. radians*	6.1×10^5	5.02
Point 1 Boulogne	2022–07–11	1.548	50.753	*Cryptophyceae*	1.4×10^5	3.46
Point 1 Boulogne	2022–07–26	1.548	50.753	*Chaetoceros*	7.4×10^4	1.6
Point 1 Boulogne	2022–08–10	1.548	50.753	*Cryptophyceae*	2.2×10^5	2.88
Wimereux SOMLIT Point C	2012–05–23	1.521	50.687	*Guinardia delicatula*	3.1×10^5	3.73
Wimereux SOMLIT Point C	2012–06–05	1.521	50.687	*Leptocylindrus (autres)*	3.4×10^5	2.12
Wimereux SOMLIT Point C	2012–06–21	1.521	50.687	*Leptocylindrus (autres)*	3.6×10^5	0.5
Wimereux SOMLIT Point C	2012–07–04	1.521	50.687	*Rhizosolenia imbricata + styliformis*	1.4×10^5	7.96
Wimereux SOMLIT Point C	2012–07–23	1.521	50.687	*Leptocylindrus (autres)*	3.2×10^5	7.87
Wimereux SOMLIT Point C	2013–05–27	1.521	50.687	*Phaeocystis*	1.2×10^6	1.94

https://doi.org/10.5194/egusphere-2025-6235
Preprint. Discussion started: 12 January 2026

Wimereux SOMLIT Point C	2013–06–10	1.521	50.687	*Leptocylindrus (autres)*	1.0×10^6	8.08
Wimereux SOMLIT Point C	2013–06–25	1.521	50.687	*Leptocylindrus (autres)*	5.9×10^6	14.19
Wimereux SOMLIT Point C	2013–07–09	1.521	50.687	*Leptocylindrus (autres)*	3.7×10^6	5.21
Wimereux SOMLIT Point C	2013–07–22	1.521	50.687	*Leptocylindrus (autres)*	2.2×10^6	2.07
Wimereux SOMLIT Point C	2015–06–04	1.521	50.687	*Chaetoceros (autres)*	5.6×10^4	4.64
Wimereux SOMLIT Point C	2015–06–18	1.521	50.687	*Leptocylindrus (autres)*	2.3×10^5	2.85
Wimereux SOMLIT Point C	2015–07–03	1.521	50.687	*Rhizosolenia imbricata + styliformis*	6.1×10^4	7.99
Wimereux SOMLIT Point C	2015–07–15	1.521	50.687	*Rhizosolenia imbricata + styliformis*	3.2×10^4	1.33
Wimereux SOMLIT Point C	2016–05–23	1.521	50.687	*Phaeocystis*	4.0×10^6	1.92
Wimereux SOMLIT Point C	2016–06–06	1.521	50.687	*Asterionellopsis*	1.2×10^5	9.64
Wimereux SOMLIT Point C	2016–06–21	1.521	50.687	*Gymnodiniales*	3.2×10^4	8.8
Wimereux SOMLIT Point C	2016–07–06	1.521	50.687	*Chaetoceros (autres)*	3.3×10^5	5.38
Wimereux SOMLIT Point C	2016–07–21	1.521	50.687	*Chaetoceros socialis + radians*	3.0×10^6	8.48
Wimereux SOMLIT Point C	2020–05–25	1.521	50.687	*Leptocylindrus (autres)*	3.5×10^4	1.53
Wimereux SOMLIT Point C	2020–06–03	1.521	50.687	*Leptocylindrus (autres)*	1.3×10^5	4.01
Wimereux SOMLIT Point C	2020–06–23	1.521	50.687	*Leptocylindrus (autres)*	1.9×10^5	4.01
Wimereux SOMLIT Point C	2020–07–07	1.521	50.687	*Chaetoceros socialis + radians*	1.8×10^4	1.54
Wimereux SOMLIT Point C	2020–07–22	1.521	50.687	*Chaetoceros socialis + radians*	8.7×10^4	3.17

https://doi.org/10.5194/egusphere-2025-6235
Preprint. Discussion started: 12 January 2026

Wimereux SOMLIT Point C	2022–05–30	1.521	50.687	*Leptocylindrus (autres)*	9.9×10^5	3.95
Wimereux SOMLIT Point C	2022–06–15	1.521	50.687	*Leptocylindrus (autres)*	2.9×10^5	4.29
Wimereux SOMLIT Point C	2022–06–29	1.521	50.687	*Leptocylindrus (autres)*	2.9×10^5	4.23
Wimereux SOMLIT Point C	2022–07–13	1.521	50.687	*Chaetoceros curvisetus + debilis + pseudocurvisetus*	1.1×10^5	4.31

Table H2. SOMLIT observations of phytoplankton functional groups at Point C and Point L between 20 May and 10 August. Data include *Synechococcus*, picoeukaryotes, cryptophytes, and nanophytoplankton abundances (cells L^{-1}).

SOMLIT Dataset	Date	Long (° E)	Lat (° N)	*Synechococcus* (Cells L^{-1})	Picoeukaryotes (Cells L^{-1})	Cryptophytes (Cells L^{-1})	Nanophytoplankton (Cells L^{-1})
Point C	2012–05–23	1.521	50.687	2.9×10^5	4.0×10^5		9.3×10^5
Point C	2012–06–21	1.521	50.687	6.1×10^6	3.3×10^5	2.5×10^3	1.4×10^6
Point C	2012–07–04	1.521	50.687	2.2×10^6	4.4×10^5		6.2×10^5
Point C	2012–07–23	1.521	50.687	2.4×10^6	4.2×10^5	3.0×10^4	5.5×10^5
Point L	2012–05–23	1.416	50.687	8.9×10^5	6.2×10^5	2.8×10^4	7.8×10^5
Point L	2012–06–21	1.416	50.687	1.7×10^6	3.4×10^5	7.6×10^3	6.6×10^5
Point L	2012–07–04	1.416	50.687	8.8×10^6	1.4×10^6	5.0×10^3	6.5×10^5
Point L	2012–07–23	1.416	50.687	5.4×10^6	6.6×10^5	2.3×10^4	5.5×10^5
Point C	2013–05–27	1.521	50.687	7.9×10^4	3.3×10^4	8.9×10^4	5.6×10^4
Point C	2013–06–10	1.521	50.687	1.3×10^6	1.8×10^5	2.5×10^4	1.9×10^5
Point C	2013–06–25	1.521	50.687	6.2×10^5	4.0×10^5	2.5×10^4	6.0×10^4
Point C	2013–07–06	1.521	50.687	9.2×10^5	2.5×10^5	5.4×10^4	2.7×10^5
Point C	2013–07–22	1.521	50.687	1.5×10^6	5.8×10^4	1.5×10^4	1.3×10^5

https://doi.org/10.5194/egusphere-2025-6235
Preprint. Discussion started: 12 January 2026

Point L	2013–05–27	1.416	50.687	4.4×10^5	1.3×10^6	3.6×10^5	3.0×10^5
Point L	2013–06–10	1.416	50.687	1.2×10^6	1.7×10^5	2.3×10^4	1.9×10^5
Point L	2013–06–25	1.416	50.687	8.4×10^6	2.9×10^5	2.5×10^4	1.3×10^5
Point L	2013–07–22	1.416	50.687	7.3×10^6	5.5×10^5	1.7×10^4	2.3×10^5
Point C	2015–06–04	1.521	50.687	8.6×10^5		2.1×10^4	9.3×10^5
Point C	2015–06–18	1.521	50.687	1.3×10^6		2.0×10^4	1.2×10^6
Point C	2015–07–03	1.521	50.687	1.0×10^7		6.7×10^4	2.2×10^6
Point C	2015–07–15	1.521	50.687	3.6×10^6	1.4×10^6	6.7×10^4	1.1×10^6
Point L	2015–06–04	1.416	50.687	3.7×10^5		3.3×10^3	1.5×10^6
Point L	2015–06–18	1.416	50.687	8.1×10^5	3.0×10^5	8.2×10^3	1.6×10^6
Point L	2015–07–03	1.416	50.687	3.4×10^7	1.1×10^7	1.3×10^5	2.6×10^6
Point L	2015–07–15	1.416	50.687	3.6×10^6	7.9×10^5	6.1×10^4	1.0×10^6
Point C	2016–05–23	1.521	50.687	2.2×10^6		1.1×10^5	1.4×10^7
Point C	2016–06–06	1.521	50.687	9.0×10^6	1.4×10^6	1.1×10^5	1.1×10^6
Point C	2016–06–21	1.521	50.687	9.9×10^6	1.5×10^6	6.7×10^4	9.6×10^5
Point C	2016–07–06	1.521	50.687	8.6×10^6	1.2×10^6	3.4×10^6	7.7×10^5
Point C	2016–07–21	1.521	50.687	5.8×10^6	2.3×10^6	4.2×10^6	2.3×10^6
Point L	2016–05–23	1.416	50.687	1.4×10^7	3.6×10^6	1.7×10^5	2.6×10^6
Point L	2016–06–06	1.416	50.687	2.1×10^7	1.8×10^6	1.8×10^5	1.4×10^6

https://doi.org/10.5194/egusphere-2025-6235
Preprint. Discussion started: 12 January 2026

Point L	2016–07–06	1.416	50.687	1.8×10^7	4.5×10^6	1.3×10^6	1.3×10^6
Point C	2020–05–25	1.521	50.687	6.9×10^6	4.8×10^6	1.5×10^5	1.7×10^6
Point C	2020–06–03	1.521	50.687	2.5×10^5	3.0×10^5	6.1×10^4	2.0×10^6
Point C	2020–06–23	1.521	50.687	3.8×10^6	6.5×10^5	1.7×10^5	2.2×10^6
Point C	2020–07–07	1.521	50.687	2.4×10^7	5.0×10^6	1.6×10^5	4.9×10^6
Point C	2020–07–22	1.521	50.687	3.4×10^7	1.6×10^7	7.3×10^5	2.1×10^6
Point L	2020–06–03	1.416	50.687	9.5×10^5	1.0×10^6	7.9×10^4	2.8×10^6
Point L	2020–07–22	1.416	50.687	8.3×10^6	4.0×10^6	3.6×10^5	2.8×10^6
Point C	2022–05–17	1.521	50.687	3.5×10^4		3.5×10^5	1.4×10^6
Point C	2022–06–29	1.521	50.687	4.9×10^7	1.8×10^7	2.5×10^5	4.2×10^6
Point C	2022–07–13	1.521	50.687	1.4×10^7	5.7×10^6	2.2×10^5	3.8×10^6
Point L	2022–05–17	1.416	50.687	2.3×10^5		4.0×10^3	4.8×10^6
Point L	2022–06–29	1.416	50.687	1.0×10^8	2.4×10^7	5.1×10^4	2.4×10^6
Point L	2022–07–13	1.416	50.687	1.8×10^7	7.8×10^6	1.0×10^5	2.1×10^6

Data availability.

The cytometric and environmental datasets (https://doi.org/10.17882/104524; Hubert et al., 2025b), as well as phytoplankton abundance data from the SOMLIT (https://doi.org/10.17882/100323; Savoye et al., 2024) and Phytobs (https://doi.org/10.17882/85178; Lemoine et al., 2024) stations, are available through the SEANOE data repository. Meteorological data (wind speed, precipitation and direction) are provided by Météo-France and available at https://meteo.data.gouv.fr/. Hydrological data on freshwater inflow are accessible from Eau France at https://www.eaufrance.fr/.

https://doi.org/10.5194/egusphere-2025-6235
Preprint. Discussion started: 12 January 2026

Author contributions.

This work was conceptualized by FGS, UC, and HC. LFA provided DYPHYRAD data HC performed the analysis and interpreted the results with input from FGS and UC. HC wrote the first draft with the help of UC and FGS. FGS and UC secured funding and supervised HC.

Competing interests.

The contact author has declared that none of the authors has any competing interests.

Special issue statement.

This article is part of the special issue "Special issue on ocean extremes (55th International Liège Colloquium)". It is a result of the 55th International Liège Colloquium on Ocean Dynamics, Liège, Belgium, 27–30 May 2024.

Acknowledgements.

The authors wish to thank the crew of the R/V *Sepia II* (CNRS INSU, French National Oceanographic Fleet), and Zeline Hubert for the DYPHYRAD automated flow cytometry database. Finally, we thank the French national observation network SOMLIT and Phytobs within the ILICO research infrastructure for providing additional phytoplankton and environment database.

Financial support.

This research has been supported by the Région Hauts-de-France and Université du Littoral Côte d'Opale. This work is also supported by the graduate school IFSEA that benefits from a France 2030 grant (ANR-21-EXES-0011) operated by the French National Research Agency.

References

Allgeier, J. E., Rosemond, A. D., and Layman, C. A.: The frequency and magnitude of non-additive responses to multiple nutrient enrichment, J. Appl. Ecol., 48, 96–101, https://doi.org/10.1111/j.1365-2664.2010.01894.x, 2011.

Aminot, A. and Kérouel, R.: Dissolved organic carbon, nitrogen and phosphorus in the N-E Atlantic and the N-W Mediterranean with particular reference to non-refractory fractions and degradation, Deep-Sea Res. Part I Oceanogr. Res. Pap., 51, 1975–1999, https://doi.org/10.1016/j.dsr.2004.07.016, 2004.

Babin, S. M., Carton, J. A., Dickey, T. D., and Wiggert, J. D.: Satellite evidence of hurricane-induced phytoplankton blooms in an oceanic desert, J. Geophys. Res.: Oceans, 109, C03043, https://doi.org/10.1029/2003JC001938, 2004.

Barnes, M. K., Tilstone, G. H., Suggett, D. J., Widdicombe, C. E., Bruun, J., Martinez-Vicente, V., and Smyth, T. J.: Temporal variability in total, micro- and nano-phytoplankton primary production at a coastal site in the Western English Channel, Prog. Oceanogr., 137, 470–483, https://doi.org/10.1016/j.pocean.2015.04.017, 2015.

https://doi.org/10.5194/egusphere-2025-6235
Preprint. Discussion started: 12 January 2026

Barnett, M. L., Kemp, A. E. S., Hickman, A. E., and Purdie, D. A.: Shelf sea subsurface chlorophyll maximum thin layers have a distinct phytoplankton community structure, Cont. Shelf Res., 174, 140–157, https://doi.org/10.1016/j.csr.2018.12.007, 2019.

Barnett, M. L., Kemp, A. E. S., Hickman, A. E., and Purdie, D. A.: Environmental controls on the interannual variability in chlorophyll and phytoplankton community structure within the seasonal sub surface chlorophyll maximum in the western English channel, Cont. Shelf Res., 277, 105253, https://doi.org/10.1016/j.csr.2024.105253, 2024.

Bianucci, L., Balaguru, K., Smith, R. W., Leung, L. R., and Moriarty, J. M.: Contribution of hurricane-induced sediment resuspension to coastal oxygen dynamics, Sci. Rep., 8, 15740, https://doi.org/10.1038/s41598-018-33640-3, 2018.

Bonato, S., Christaki, U., Lefebvre, A., Lizon, F., Thyssen, M., and Artigas, L. F.: High spatial variability of phytoplankton assessed by flow cytometry, in a dynamic productive coastal area, in spring: The eastern English Channel, Estuar. Coast. Shelf Sci., 154, 214–223, https://doi.org/10.1016/j.ecss.2014.12.037, 2015.

Bonato, S., Breton, E., Didry, M., Lizon, F., Cornille, V., Lécuyer, E., Christaki, U., and Artigas, L. F.: Spatio-temporal patterns in phytoplankton assemblages in inshore–offshore gradients using flow cytometry: A case study in the eastern English Channel, J. Mar. Syst., 156, 76–85, https://doi.org/10.1016/j.jmarsys.2015.11.009, 2016.

Breton, E., Christaki, U., Sautour, B., Demonio, O., Skouroliakou, D.-I., Beaugrand, G., Seuront, L., Kléparski, L., Poquet, A., Nowaczyk, A., Crouvoisier, M., Ferreira, S., Pecqueur, D., Salmeron, C., Brylinski, J.-M., Lheureux, A., and Goberville, E.: Seasonal Variations in the Biodiversity, Ecological Strategy, and Specialization of Diatoms and Copepods in a Coastal System With Phaeocystis Blooms: The Key Role of Trait Trade-Offs, Front. Mar. Sci., 8, 656300, https://doi.org/10.3389/fmars.2021.656300, 2021.

Brunet, C., Brylinski, J. M., Bodineau, L., Thoumelin, G., Bentley, D., and Hilde, D.: Phytoplankton Dynamics During the Spring Bloom in the South-eastern English Channel, Estuar. Coast. Shelf Sci., 43, 469–483, https://doi.org/10.1006/ecss.1996.0082, 1996.

Brylinski, J. M., Lagadeuc, Y., Gentilhomme, V., Dupont, J. P., Lafite, R., Dupeuble, P. A., Huault, M. F., Auger, Y., Puskaric, E., Wartel, M., and Cabioch, L.: Le “fleuve côtier”: Un phénomène hydrologique important en Manche orientale. Exemple du Pas-de-Calais, Oceanol. Acta, 11, 197–203, 1991.

Brylinski, J. M., Brunet, C., Bentley, D., Thoumelin, G., and Hilde, D.: Hydrography and Phytoplankton Biomass in the Eastern English Channel in Spring 1992, Estuar. Coast. Shelf Sci., 43, 507–519, https://doi.org/10.1006/ecss.1996.0084, 1996.

Carpenter, S. R., Gahler, M. R., Kucharik, C. J., and Stanley, E. H.: Long-range dependence and extreme values of precipitation, phosphorus load, and Cyanobacteria, Proc. Natl. Acad. Sci. U.S.A., 119, e2214343119, https://doi.org/10.1073/pnas.2214343119, 2022.

Cook, E. R., Seager, R., Kushnir, Y., Briffa, K. R., Büntgen, U., Frank, D., Krusic, P. J., Tegel, W., Van Der Schrier, G., Andreu-Hayles, L., Baillie, M., Baittinger, C., Bleicher, N., Bonde, N., Brown, D., Carrer, M., Cooper, R., Čufar, K., Dittmar, C., Esper, J., Griggs, C., Gunnarson, B., Günther, B., Gutierrez, E., Haneca, K., Helama, S., Herzig, F., Heussner, K.-U., Hofmann, J., Janda, P., Kontic, R., Köse, N., Kyncl, T., Levanič, T., Linderholm, H., Manning, S., Melvin, T. M., Miles, D., Neuwirth, B., Nicolussi, K., Nola, P., Panayotov, M., Popa, I., Rothe, A., Seftigen, K., Seim, A., Svarva, H., Svoboda, M., Thun, T., Timonen, M., Touchan, R., Trotsiuk, V., Trouet,

https://doi.org/10.5194/egusphere-2025-6235
Preprint. Discussion started: 12 January 2026

V., Walder, F., Ważny, T., Wilson, R., and Zang, C.: Old World megadroughts and pluvials during the Common Era, Sci. Adv., 1, e1500561, https://doi.org/10.1126/sciadv.1500561, 2015.

Crawford, A. D., Krumhardt, K. M., Lovenduski, N. S., Van Dijken, G. L., and Arrigo, K. R.: Summer High-Wind Events and Phytoplankton Productivity in the Arctic Ocean, J. Geophys. Res.: Oceans, 125, e2020JC016565, https://doi.org/10.1029/2020JC016565, 2020.

Crawford, A. D., McCrystall, M. R., Lukovich, J. V., and Stroeve, J. C.: The Response of Extratropical Cyclone Propagation in the Northern Hemisphere to Global Warming, J. Climate, 36, 7123–7142, https://doi.org/10.1175/JCLI-D-23-0082.1, 2023.

Derot, J., Schmitt, F. G., Gentilhomme, V., and Zongo, S. B.: Long-term high frequency phytoplankton dynamics, recorded from a coastal water autonomous measurement system in the eastern English Channel, Cont. Shelf Res., 109, 210–221, https://doi.org/10.1016/j.csr.2015.09.015, 2015.

Dietze, M., Bell, R., Ozturk, U., Cook, K. L., Andermann, C., Beer, A. R., Damm, B., Lucia, A., Fauer, F. S., Nissen, K. M., Sieg, T., and Thieken, A. H.: More than heavy rain turning into fast-flowing water – a landscape perspective on the 2021 Eifel floods, Nat. Hazards Earth Syst. Sci., 22, 1845–1856, https://doi.org/10.5194/nhess-22-1845-2022, 2022.

Dulière, V., Gypens, N., Lancelot, C., Luyten, P., and Lacroix, G.: Origin of nitrogen in the English Channel and Southern Bight of the North Sea ecosystems, Hydrobiologia, 845, 13–33, https://doi.org/10.1007/s10750-017-3419-5, 2019.

Francis, J. A., Skific, N., and Vavrus, S. J.: Increased persistence of large-scale circulation regimes over Asia in the era of amplified Arctic warming, past and future, Sci. Rep., 10, 14953, https://doi.org/10.1038/s41598-020-71945-4, 2020.

Gieskes, W. W. C., Leterme, S. C., Peletier, H., Edwards, M., and Reid, P. C.: Phaeocystis colony distribution in the North Atlantic Ocean since 1948, and interpretation of long-term changes in the Phaeocystis hotspot in the North Sea, Biogeochemistry, 83, 49–60, https://doi.org/10.1007/s10533-007-9082-6, 2007.

Gronholz, A., Gräwe, U., Paul, A., and Schulz, M.: Investigating the effects of a summer storm on the North Sea stratification using a regional coupled ocean-atmosphere model, Ocean Dyn., 67, 211–235, https://doi.org/10.1007/s10236-016-1023-2, 2017.

Guinaldo, T., Voldoire, A., Waldman, R., Saux Picart, S., and Roquet, H.: Response of the sea surface temperature to heatwaves during the France 2022 meteorological summer, Ocean Sci., 19, 629–647, https://doi.org/10.5194/os-19-629-2023, 2023.

Helton, J. C.: Uncertainty and sensitivity analysis in the presence of stochastic and subjective uncertainty, J. Stat. Comput. Simul., 57, 3–76, https://doi.org/10.1080/00949659708811803, 1997.

Houliez, E., Schmitt, F. G., Breton, E., Skouroliakou, D.-I., and Christaki, U.: On the conditions promoting Pseudo-nitzschia spp. blooms in the eastern English Channel and southern North Sea, Harmful Algae, 125, 102424, https://doi.org/10.1016/j.hal.2023.102424, 2023.

Hubert, Z., Louchart, A. P., Robache, K., Epinoux, A., Gallot, C., Cornille, V., Crouvoisier, M., Monchy, S., and Artigas, L. F.: Decadal changes in phytoplankton functional composition in the Eastern English Channel: possible upcoming major effects of climate change, Ocean Sci., 21, 679–700, https://doi.org/10.5194/os-21-679-2025, 2025a.

https://doi.org/10.5194/egusphere-2025-6235
Preprint. Discussion started: 12 January 2026

Hubert, Z., Libeau, A., Gallot, C., and Artigas, L. F.: Dynamics of phytoplankton on RADiale of the Saint-Jean Bay (DYPHYRAD) surveys, SEANOE [data set], https://doi.org/10.17882/104524, 2025b.

Hubert, Z., Libeau, A., Gallot, C., Cornille, V., Crouvoisier, M., Lecuyer, E., and Artigas, L. F.: Phytoplankton coastal-offshore monitoring by the Strait of Dover at high spatial resolution: the DYPHYRAD surveys, Earth Syst. Sci. Data Discuss. [preprint], https://doi.org/10.5194/essd-2025-131, in review, 2025c.

Huguet, A., Barillé, L., Soudant, D., Petitgas, P., Gohin, F., and Lefebvre, A.: Identifying the spatial pattern and the drivers of the decline in the eastern English Channel chlorophyll-a surface concentration over the last two decades, Mar. Pollut. Bull., 199, 115870, https://doi.org/10.1016/j.marpolbul.2023.115870, 2024.

Jacobsen, B. A. and Simonsen, P.: Disturbance events affecting phytoplankton biomass, composition and species diversity in a shallow, eutrophic, temperate lake, Hydrobiologia, 249, 9–14, https://doi.org/10.1007/BF00008838, 1993.

Jena, B., Swain, D., and Avinash, K.: Investigation of the biophysical processes over the oligotrophic waters of South Indian Ocean subtropical gyre, triggered by cyclone Edzani, Int. J. Appl. Earth Obs. Geoinf., 18, 49–56, https://doi.org/10.1016/j.jag.2012.01.006, 2012.

Jennings, E., Jones, S., Arvola, L., Staehr, P. A., Gaiser, E., Jones, I. D., Weathers, K. C., Weyhenmeyer, G. A., Chiu, C., and De Eyto, E.: Effects of weather-related episodic events in lakes: an analysis based on high-frequency data, Freshw. Biol., 57, 589–601, https://doi.org/10.1111/j.1365-2427.2011.02729.x, 2012.

Jurburg, S. D., Nunes, I., Stegen, J. C., Le Roux, X., Priemé, A., Sørensen, S. J., and Salles, J. F.: Autogenic succession and deterministic recovery following disturbance in soil bacterial communities, Sci. Rep., 7, 45691, https://doi.org/10.1038/srep45691, 2017.

Kaspi, Y. and Schneider, T.: The Role of Stationary Eddies in Shaping Midlatitude Storm Tracks, J. Atmos. Sci., 70, 2596–2613, https://doi.org/10.1175/JAS-D-12-082.1, 2013.

Kasprzak, P., Shatwell, T., Gessner, M. O., Gonsiorczyk, T., Kirillin, G., Selmeczy, G., Padisák, J., and Engelhardt, C.: Extreme Weather Event Triggers Cascade Towards Extreme Turbidity in a Clear-water Lake, Ecosystems, 20, 1407–1420, https://doi.org/10.1007/s10021-017-0121-4, 2017.

Kuczynska, P., Jemiola-Rzeminska, M., and Strzalka, K.: Photosynthetic Pigments in Diatoms, Mar. Drugs, 13, 5847–5881, https://doi.org/10.3390/md13095847, 2015.

Lamy, D., Obernosterer, I., Laghdass, M., Artigas, F., Breton, E., Grattepanche, J., Lecuyer, E., Degros, N., Lebaron, P., and Christaki, U.: Temporal changes of major bacterial groups and bacterial heterotrophic activity during a Phaeocystis globosa bloom in the eastern English Channel, Aquat. Microb. Ecol., 58, 95–107, https://doi.org/10.3354/ame01359, 2009.

Lefebvre, A., Guiselin, N., Barbet, F., and Artigas, F. L.: Long-term hydrological and phytoplankton monitoring (1992–2007) of three potentially eutrophic systems in the eastern English Channel and the Southern Bight of the North Sea, ICES J. Mar. Sci., 68, 2029–2043, https://doi.org/10.1093/icesjms/fsr149, 2011.

Lemoine, M., Claquin, P., Eric, A., Christophe, A., Artigas, F. L., Hadrien, B., Belin, C., Blondel, C., Breton, E., Caillard, E., Carpentier, L., Chomerat, N., Christaki, U., Conan, P., Cornet, V., Coste, L., Courtay, G., Courtois, B., Dagault, F., Del amo, Y., Delebecq, G., Doner, A., Dupuy, C., Fauchot, J., Francoise, S., Gabellec, R., Hernandez, F. T., Klein, C., Lampert, L., Le Roy, B., Lebon, F., Lefebvre, A., Legendre, A., Lejolivet, A., Lemée, R., Leynaert, A., Manach, S., Marro, S., Menet-Nedelec, F., Mertens, K., Meteigner, C., Marco-Miralles, F., Neaud-Masson, N., Nezan, E., Perriere-Rumebe, M., Queguiner, B., Retho, M., Rigaut-Jalabert, F., Sauriau, P.-

https://doi.org/10.5194/egusphere-2025-6235
Preprint. Discussion started: 12 January 2026

G., Schapira, M., Serais, O., Simon, N., Vidussi, F., Vuillemin, R., Auby, I., Beker, B., Breret, M., Chabirand, J.-M., Chiantella, C., Crispi, O., Deton-Cabanillas, A.-F., Duquesne, V., Duval, A., Fiandrino, A., Genauzeau, S., Gle, C., Guesdon, S., Guilloux, L., Pascale, H., Benoist, H., Auriane, J., Labatut, P., Yann, L., Pascale, M., Eric, M., Mas, S., Mostajir, B., Rene, O., Pineau, P., Piraud, A., Ryckaert, M., Schmitt, A., Thorel, M., Vaulot, D., Viprey, M., Bergeret, J., Foulon, E., Gourvil, P., Le Gall, F., Lebrun, L., Not, F., Ristori, S., Terre-Terrillon, A., Hoebeke, M., Rouilly, A., and Siltanen, J.: PHYTOBS dataset - French National Service of Observation for Phytoplankton in coastal waters, SEANOE [data set], https://doi.org/10.17882/85178, 2024.

Litchman, E., Klausmeier, C. A., and Yoshiyama, K.: Contrasting size evolution in marine and freshwater diatoms, Proc. Natl. Acad. Sci. U.S.A., 106, 2665–2670, https://doi.org/10.1073/pnas.0810891106, 2009.

Loquet, N., Rybarczyk, H., and Elkaim, B.: Échanges de sels nutritifs entre la zone côtière et un système estuarien intertidal : la baie de Somme (Manche, France), Oceanol. Acta, 2000.

Lorenzen, C. J.: A method for the continuous measurement of in vivo chlorophyll concentration, Deep Sea Research and Oceanographic Abstracts, 13, 223–227, https://doi.org/10.1016/0011-7471(66)91102-8, 1966.

Louchart, A., Lizon, F., Lefebvre, A., Didry, M., Schmitt, F. G., and Artigas, L. F.: Phytoplankton distribution from Western to Central English Channel, revealed by automated flow cytometry during the summer-fall transition, Cont. Shelf Res., 195, 104056, https://doi.org/10.1016/j.csr.2020.104056, 2020.

Margalef, R.: Life-forms of phytoplankton as survival alternatives in an unstable environment, Oceanol. Acta, 4, 493–509, 1978.

Pfleiderer, P., Schleussner, C.-F., Kornhuber, K., and Coumou, D.: Summer weather becomes more persistent in a 2 °C world, Nat. Clim. Chang., 9, 666–671, https://doi.org/10.1038/s41558-019-0555-0, 2019.

Pniewski, F. and Piasecka-Jędrzejak, I.: Photoacclimation to Constant and Changing Light Conditions in a Benthic Diatom, Front. Mar. Sci., 7, 381, https://doi.org/10.3389/fmars.2020.00381, 2020.

Pozdnyakov, D., Tang, D., Bobylev, L., Golubkin, P., Zabolotskikh, E., Petrenko, D., and Morozov, E.: A Pilot Satellite-Based Investigation of the Impact of a Deep Polar Cyclone Propagation on the Phytoplankton Chlorophyll Spatial and Temporal Dynamics in the Arctic Ocean, in: Typhoon Impact and Crisis Management, vol. 40, edited by: Tang, D. L. and Sui, G., Springer, Berlin, Heidelberg, Germany, 241–251, https://doi.org/10.1007/978-3-642-40695-9_11, 2014.

Priestley, M. D. K. and Catto, J. L.: Future changes in the extratropical storm tracks and cyclone intensity, wind speed, and structure, Weather Clim. Dynam., 3, 337–360, https://doi.org/10.5194/wcd-3-337-2022, 2022.

Priestley, M. D. K., Ackerley, D., Catto, J. L., Hodges, K. I., McDonald, R. E., and Lee, R. W.: An Overview of the Extratropical Storm Tracks in CMIP6 Historical Simulations, J. Climate, 33, 6315–6343, https://doi.org/10.1175/JCLI-D-19-0928.1, 2020.

Raven, J. A.: A Cost-Benefit Analysis of Photon Absorption by Photosynthetic Unicells, New Phytol., 98, 593–625, https://doi.org/10.1111/j.1469-8137.1984.tb04152.x, 1984.

Rees, A. P., Hope, S. B., Widdicombe, C. E., Dixon, J. L., Woodward, E. M. S., and Fitzsimons, M. F.: Alkaline phosphatase activity in the western English Channel: Elevations induced by high summertime rainfall, Estuar. Coast. Shelf Sci., 81, 569–574, https://doi.org/10.1016/j.ecss.2008.12.005, 2009.

Robache, K., Hubert, Z., Gallot, C., Epinoux, A., Louchart, A. P., Facq, J.-V., Lefebvre, A., Répécaud, M., Cornille, V., Verhaeghe, F., Audinet, Y., Brutier, L., Schmitt, F. G., and Artigas, L. F.: Multiscale phytoplankton

https://doi.org/10.5194/egusphere-2025-6235
Preprint. Discussion started: 12 January 2026

dynamics in a coastal system of the eastern English Channel: the Boulogne-sur-Mer coastal area, Ocean Sci., 21, 1787–1811, https://doi.org/10.5194/os-21-1787-2025, 2025.

Savoye, N., Lizon, F., Breton, E., Claquin, P., Joly, O., Sultan, E., Jung, J.-L., Bozec, Y., Boulart, C., Rimmelin-Maury, P., Leynaert, A., Agogué, H., Pineau, P., Del Amo, Y., Conan, P., Mostajir, B., Grégori, G., Mousseau, L., and Mendès, F.: SOMLIT (Service d'Observation en Milieu Littoral) time series (French Research Infrastructure ILICO): long-term core parameter monitoring of French coasts, SEANOE [data set], https://doi.org/10.17882/100323, 2024.

Schmitt, F. G., Jiang, Y., Lecuyer, E., Crouvoisier, M., Berti, S., Calzavarini, E., Tergolina, V., and Mayette, E.: Stratification thermique des eaux marines au large de Boulogne-sur-mer, in: Observer le monde marin, de la ressource à l'assiette : recherches marines et littorales en Côte d'Opale, Editions Universitaires Européennes, 295–306, ISBN : 978-3-8416-7831-7, 2024.

Scholz, S. R., Seager, R., Ting, M., Kushnir, Y., Smerdon, J. E., Cook, B. I., Cook, E. R., and Baek, S. H.: Changing hydroclimate dynamics and the 19th to 20th century wetting trend in the English Channel region of northwest Europe, Clim. Dyn., 58, 1539–1553, https://doi.org/10.1007/s00382-021-05977-5, 2022.

Simon, A., Poppeschi, C., Plecha, S., Charria, G., and Russo, A.: Coastal and regional marine heatwaves and cold spells in the northeastern Atlantic, Ocean Sci., 19, 1339–1355, https://doi.org/10.5194/os-19-1339-2023, 2023.

Skouroliakou, D.-I., Breton, E., Irion, S., Artigas, L. F., and Christaki, U.: Stochastic and Deterministic Processes Regulate Phytoplankton Assemblages in a Temperate Coastal Ecosystem, Microbiol. Spectr., 10, e02427-22, https://doi.org/10.1128/spectrum.02427-22, 2022.

Stockwell, J. D., Doubek, J. P., Adrian, R., Anneville, O., Carey, C. C., Carvalho, L., De Senerpont Domis, L. N., Dur, G., Frassl, M. A., Grossart, H., Ibelings, B. W., Lajeunesse, M. J., Lewandowska, A. M., Llames, M. E., Matsuzaki, S. S., Nodine, E. R., Nõges, P., Patil, V. P., Pomati, F., Rinke, K., Rudstam, L. G., Rusak, J. A., Salmaso, N., Seltmann, C. T., Straile, D., Thackeray, S. J., Thiery, W., Urrutia-Cordero, P., Venail, P., Verburg, P., Woolway, R. I., Zohary, T., Andersen, M. R., Bhattacharya, R., Hejzlar, J., Janatian, N., Kpodonu, A. T. N. K., Williamson, T. J., and Wilson, H. L.: Storm impacts on phytoplankton community dynamics in lakes, Glob. Change Biol., 26, 2756–2784, https://doi.org/10.1111/gcb.15033, 2020.

Thyssen, M., Grégori, G. J., Grisoni, J.-M., Pedrotti, M. L., Mousseau, L., Artigas, L. F., Marro, S., Garcia, N., Passafiume, O., and Denis, M. J.: Onset of the spring bloom in the northwestern Mediterranean Sea: influence of environmental pulse events on the in situ hourly-scale dynamics of the phytoplankton community structure, Front. Microbiol., 5, 387, https://doi.org/10.3389/fmicb.2014.00387, 2014.

Thyssen, M., Grégori, G., Créach, V., Lahbib, S., Dugenne, M., Aardema, H. M., Artigas, L.-F., Huang, B., Barani, A., Beaugeard, L., Bellaaj-Zouari, A., Beran, A., Casotti, R., Del Amo, Y., Denis, M., Dubelaar, G. B. J., Endres, S., Haraguchi, L., Karlson, B., Lambert, C., Louchart, A., Marie, D., Moncoiffé, G., Pecqueur, D., Ribalet, F., Rijkeboer, M., Silovic, T., Silva, R., Marro, S., Sosik, H. M., Sourisseau, M., Tarran, G., Van Oostende, N., Zhao, L., and Zheng, S.: Interoperable vocabulary for marine microbial flow cytometry, Front. Mar. Sci., 9, 975877, https://doi.org/10.3389/fmars.2022.975877, 2022.

Wasko, C., Nathan, R., Stein, L., and O'Shea, D.: Evidence of shorter more extreme rainfalls and increased flood variability under climate change, J. Hydrol., 603, 126994, https://doi.org/10.1016/j.jhydrol.2021.126994, 2021.

https://doi.org/10.5194/egusphere-2025-6235
Preprint. Discussion started: 12 January 2026

Williams, C., Sharples, J., Mahaffey, C., and Rippeth, T.: Wind-driven nutrient pulses to the subsurface chlorophyll maximum in seasonally stratified shelf seas, Geophys. Res. Lett., 40, 5467–5472, https://doi.org/10.1002/2013GL058171, 2013.

Wu, J.: Wind-stress coefficients over sea surface from breeze to hurricane, J. Geophys. Res., 87, 9704–9706, https://doi.org/10.1029/JC087iC12p09704, 1982.

Xian, W.-D., Ding, J., Chen, J., Qu, W., Cao, P., Tang, C., Liu, X., Zhang, Y., Li, J.-L., Wang, P., Li, W.-J., and Wang, J.: Distinct Assembly Processes Structure Planktonic Bacterial Communities Among Near- and Offshore Ecosystems in the Yangtze River Estuary, Microb. Ecol., 87, 42, https://doi.org/10.1007/s00248-024-02350-x, 2024.

Zhao, H., Tang, D., and Wang, D.: Phytoplankton blooms near the Pearl River Estuary induced by Typhoon Nuri, J. Geophys. Res., 114, 2009JC005384, https://doi.org/10.1029/2009JC005384, 2009.